ENHANCEMENT OF POOL BOILING AND EVAPORATIVE HEAT TRANSFER USING HIGH TEMPERATURE THERMALLY CONDUCTIVE MICROPOROUS COATINGS

by

AJAY GURUNG

Presented to the Faculty of the Graduate School of

The University of Texas at Arlington in Partial Fulfillment

of the Requirements

for the Degree of

DOCTOR OF PHILOSOPHY

THE UNIVERSITY OF TEXAS AT ARLINGTON

December 2014

ACKNOWLDEGEMENTS

I would like to express my deepest appreciation and gratitude to my parents Maya Gurung (mother), and Yam Bahadur Gurung (father), for their unconditional love and support throughout my whole life. I would like to dedicate this document to them. I would also like to thank my siblings: Mira Gurung and Bijaya Gurung, for their encouragement.

My utmost appreciation also goes to my supervising professor Dr. Hyejin Moon and to Dr. Seung M. You for their guidance throughout my research activities. Countless suggestions and help from Dr. Miguel Amaya is also very much appreciated. I would like to thank all my current and former lab members for their support and friendship.

Finally, I would like to thank my wife, Chandani Rana, for her unending love and support. She always believed in me, even when I doubted myself. I have been truly blessed with the most wonderful wife a man could have.

October 31, 2014

ABSTRACT

ENHANCEMENT OF POOL BOILING AND EVAPORATIVE HEAT TRANSFER USING HIGH TEMPERATURE THERMALLY CONDUCTIVE MICROPOROUS COATINGS

Ajay Gurung, PhD

The University of Texas at Arlington, 2014

Supervising Professor: Hyejin Moon

The present research is an experimental study of the enhancement of pool boiling and evaporative heat transfer using high temperature thermally conductive microporous coatings. Two major types of coatings were investigated: one that is based on copper powders on copper substrate and the other on aluminum powders on aluminum substrate. Both coatings were easy to fabricate with low costs compared to conventional sintering and plasma spraying techniques, yet have high bonding strength and some of them can operate at temperatures up to 670 ^{o}C. Multiple coating options were fabricated and tested in pool boiling of water in order to optimize the coating. These coating options consisted of variations of coating composition ratio, coating thickness and powder sizes. Average powder sizes ranged from 5 µm to 110 µm, and coating thicknesses from 75 µm to 340 µm, applied on flat 1x1cm^2 test heaters. The heaters were tested in the horizontal, upward-facing orientation in saturated conditions at atmospheric pressure and under increasing heat flux. Pool boiling results revealed an optimum composition, powder size and thickness for each coating types. The maximum enhancement in boiling heat transfer coefficient obtained from copper microporous coatings was up to 8.7 times relative to a plain copper test surface and nearly doubled the critical heat flux while aluminum microporous coatings enhanced boiling heat transfer coefficient by 3.5 times compared to plain aluminum surface without any further enhancement in CHF. This enhancement was ascribed to the numerous microcavities of optimum shape and size formed within the

porous matrix of the coating. The detail microstructures of the coatings from the top surface as well as cross-sections are also presented through optical microscope and SEM images. The optimized aluminum coatings were also explored on fluids other than water such as acetone and HFE-7100 for their boiling heat transfer enhancement. Furthermore, the same coatings were applied on evaporative spray and jet-impingement tests using water to broaden the application of aluminum microporous coatings in evaporative cooling technology.

TABLE OF CONTENTS

LIST OF ILLUSTRATIONS

LIST OF TABLES

NOMENCLATURE

k	thermal conductivity, [W/m.K]
c_p	specific heat capacity, [J/kg-K]
g	gravitational acceleration, [m/s^2]
r	radius, [µm]
h_{lv}	latent heat of vaporization, [J/kg]
Nu	Nusselt number
Pr	Prandtl number
We	Weber number
Re	Reynolds number
q''	heat flux, [W/cm^2]
Ra	Rayleigh number
P	pressure, [kPa]
T	temperature, [°C]
V	volume of bubbles, [m^3]
SMD	sauted mean diameter, [µm]

Greek Symbols

ρ	density, [kg/m^3]
σ	surface tension, [N/m]
α	heat transfer coefficient [[W/m^{2}K]
μ	dynamic viscosity, [kg/m.s]
Ω	Ohm
ΔT_{sat}	wall superheat, T_w-T_{sat}(P_{sys})

Subscripts

a	air
b	bubble
v	vapor (saturated)
l	liquid (saturated)
w	heater surface (wall)
z	Zuber’s prediction
Cu	copper
Al	Aluminum
crit	critical
inc	incipience
nb	nucleate boiling
bulk	bulk quantity
CHF	critical heat flux

CHAPTER 1

INTRODUCTION

1.1 Background and Motivation

Relentless increase in spatial density of microelectronic devices has driven the rise of integrated circuit chip powers for decades and as a consequence the need of dissipating high heat flux from such devices has never been more challenging. Failure to effectively dissipate the heat generated from the chips can lead to poor performance, reliability concerns, reduced operational lifetimes, and sometimes even safety risk. In order to make sure that the electronic devices be reliable and deliver their highest performances, they must be kept under the operating temperature limit. The traditional approaches using natural convection and forced-air or liquid cooling are becoming less viable as power levels increase. Therefore, two-phase (liquid-vapor) heat transfer can be a viable alternative because of its high heat transfer rates resulting from fluid's latent heat of vaporization and isothermal characteristics of phase change process itself.

Most-recognized two-phase heat transfer cooling schemes that have seen a resurgence in interest in thermal management applications are nucleate boiling (pool and flow boiling), and evaporative (spray and jet impingement) cooling. Nucleate pool boiling has been used in immersion cooling, where the heated structure is immersed in a pool of liquid. This process is not limited to microelectronics cooling but can also be found in a variety of other industries, including nuclear and non-nuclear power generation. For an example, spent fuel rods in a nuclear reactor plant, which are at extremely high temperature, are generally placed in a pool of water for cooling. This process can be enhanced by nucleate boiling. Flow boiling has been employed in microchannel heat sink, while vapor chambers, heat pipes and other heat exchanger devices have used evaporation as primary mode of heat transfer.

The ubiquity of two-phase heat transfer systems across numerous industries and engineering applications calls for investigations to further enhance the phase change mechanisms. Typically in a two-

phase heat transfer system, where heat is transferred from a source through a surface to a working fluid, the system's ability to transfer heat energy is characterized by the behavior of the liquid at the surface-liquid interface. Thus, it is highly desirable to engineer the heat transfer surface to promote efficient boiling and evaporation, specifically nucleate boiling heat transfer.

Due to importance of enhanced surfaces, the engineering community has made great strides in phase change enhancement through a long history of surface engineering. An extensive literature survey for boiling enhancement by surface engineering is provided in CHAPTER 1.4. Through the years, UTA Microscale Heat Transfer Lab has been the pioneer in developing several microporous coatings [1] [2] [3] by particle layering technique that stand out for their simplicity in fabrication and yet when applied to heated surfaces for boiling (pool, and flow) tests, have demonstrated significant enhancement to the heat transfer coefficients, critical heat flux (CHF) and boiling incipience. The earliest microporous coating developed in the lab, known as ABM, has shown nucleate boiling heat transfer enhancement, mostly for varieties of refrigerants and has already been tested in many applications such as microelectronics cooling [4] and two-phase microchannel heat sink [5]. However, ABM is ineffective when the working fluid is water due to its smaller particles and non-conductive epoxy [3] and can be ruined if the surface temperature approaches 130 ^{o}C or more. In order to overcome these limitations, Kim [3] developed a thermally conductive microporous coating (TCMC) which is composed entirely of thermally (metallic) conductive components. TCMC significantly improved heat transfer performance of not only pool boiling of water [3], but also of flow boiling and spray cooling of FC fluids [6]. Unfortunately, when used with water, this coating became unreliable due to galvanic corrosion potential between copper and tin (solder). Corrosion produces non-condensable gas, which is typically detrimental to the performance of sealed systems, such as vapor chamber or heat pipes. More importantly, TCMC cannot be used in the applications where surface temperature is expected to be more than 200 ^{o}C as the solder used in TCMC melts at that temperature. An example of such high temperature application would be the cooling system in the nuclear reactors, where water is boiled at high pressure (~15 MPa), and the boiling point of water is ~350 ^{o}C. Sintered microporous

coatings developed outside UTA Microscale Heat Transfer Lab [7] [8] can withstand high temperature, but require complex fabrication skill and high cost equipment. Sintering needs high pressure press for compacting, high temperature furnace above 1000 ^{o}C, and vacuum environment if not expensive inert gas such as Hydrogen. In addition to the high cost, most of the sintered coatings reported have been used with wetting fluids, in which case high heat flux cooling cannot be achieved because of the low h_{fg} of such fluids. Only few of them are reported for use with water, which is more appropriate fluid for high heat flux cooling. Therefore, a novel microporous coating, which is thermally conductive, high temperature applicable, and doesn't compromise cost-effective fabrication, is needed for the boiling enhancement of water, specifically for high heat flux cooling.

1.2 Project Objectives

In the present study, the main effort is to develop another thermally conductive copper micro-porous coating which uses simple, and economic technique similar to ABM, appropriate for improvement of nucleate boiling heat transfer of water, and overcomes the temperature limitation of TCMC, as well as eliminates its galvanic corrosion potential. The coating is fabricated by using brazing technique and then optimized in its composition, thickness and particle size in order to maximize boiling heat transfer coefficient for water.

Cooling devices in aerospace industries such as cold plates, heat exchangers, heat sinks, vapor chamber and heat pipes are often made of aluminum because of its low cost, low weight and better machinability. However, using porous material dissimilar from aluminum on top of aluminum substrate, to enhance two phase heat transfer, can reduce reliability because of the potential galvanic corrosion. Moreover, soldering is difficult on aluminum and sintering of copper particles requires temperatures above the melting point of aluminum itself (660 ^{o}C). Therefore, in this study, another thermally conductive micro-porous coating is developed using aluminum particles and brazing technique. Like Cu-HTCMC, this coating

is also optimized for the composition, thickness and powder size in order to achieve the best boiling performance.

Since acetone and refrigerants, such as HFE-7100, are commonly used with aluminum heat exchanger devices, Al-HTCMC is tested in these two fluids. As their properties, such as surface tension, are different than water, it is important to identify the optimal particle size of Al-HTCMC for these fluids. Therefore, three different powder sizes are tested in the study of pool boiling heat transfer enhancement for acetone and HFE-7100. In addition, Al-HTCMC, when treated with hot water, exhibits suitable surface properties for evaporative heat transfer such as wetting and spreading of water to form thin liquid film. While increasing the heat transfer area, microcavities of the Al-HTCMC are also known to promote nucleation. Therefore, Al-HTCMC coating optimized from pool boiling tests is used to enhance spray and jet-impingement cooling performance of water.

The overall goals and objectives of this study are listed below.

1. Investigate pool boiling heat transfer enhancement of saturated water using copper micro-porous coating (Cu-HTCMC) and aluminum micro-porous coating (Al-HTCMC)
    1.1. Develop high temperature, thermally conductive, copper and aluminum micro-porous coatings by brazing technique
    1.2. Maximize the enhancement of nucleate pool boiling heat transfer for saturated water by optimizing the coating's composition (powder to brazing paste ratio), thickness, and powder size
    1.3. Compare the nucleate pool boiling performance of Cu-HTCMC and Al-HTCMC with other microporous coatings used in water
2. Investigate pool boiling heat transfer enhancement of saturated acetone and HFE-7100 using aluminum micro-porous coating
    2.1. Quantify enhancement of the heat transfer coefficients and critical heat flux
    2.2. Identify the optimal particle size of Al-HTCMC for acetone and HFE-7100
3. Investigate the application of Al-HTCMC for evaporative heat transfer enhancement

3.1. Enhancement of spray cooling using Al-HTCMC

3.2. Enhancement of jet-impingement cooling using Al-HTCMC

1.3 Fundamentals of Pool Boiling Heat Transfer

Pool boiling heat transfer refers to heat being transferred from a surface to liquid macroscopically at rest. This can be most easily understood through introduction of a boiling curve, as shown in Figure 1.1. A typical boiling curve is a plot of heat flux q" versus wall superheat, the temperature difference between the heater surface and the bulk fluid. There are distinct regimes in a boiling curve, each depicting the behavior of the boiling system. At low heat flux, heat is transferred to the liquid via natural convection. In this regime, the temperature of the liquid immediately adjacent to the heater surface increases, thereby lowering its density, causing it to rise due to buoyancy forces. In Figure 1.1, this region is from point A to point B.

Increasing heat flux eventually results in the onset of nucleate boiling (point B), where vapor bubbles start to emerge from the heated surface. Heat flux at this point is generally referred as incipience heat flux, $q"_{inc}$. As nucleate boiling requires a large heat of vaporization for the phase change during bubble formation, a significant amount of heat is removed from the heated surface. Therefore, the surface temperature doesn't rise as fast with increasing heat flux in this regime. Initially in the nucleate boiling regime (point C to point D), the bubbles are isolated due to fewer and widely separated active nucleation sites. As the heat flux increases, the number of active sites becomes so dense that adjacent bubbles merge together forming vapor slugs and columns. This regime is represented from point D to point E in Figure 1.1. Eventually, as the heat flux is driven upward, the surface is hot enough to sustain a stable vapor film on the surface. The vapor film then blankets the entire heated surface and liquid cannot reach the heated surface on time resulting in a large temperature spike. There is a sharp drop in heat transfer coefficient, occurring at point E; this is known as critical heat flux (CHF). Generally, CHF is the limiting factor for real applications

due to the significant increase in surface temperature. After the point of CHF in the boiling curve, if the heat flux remains constant, the system will transition to the film boiling regime, which exhibits much worse heat transfer coefficient compared to nucleate boiling regime.

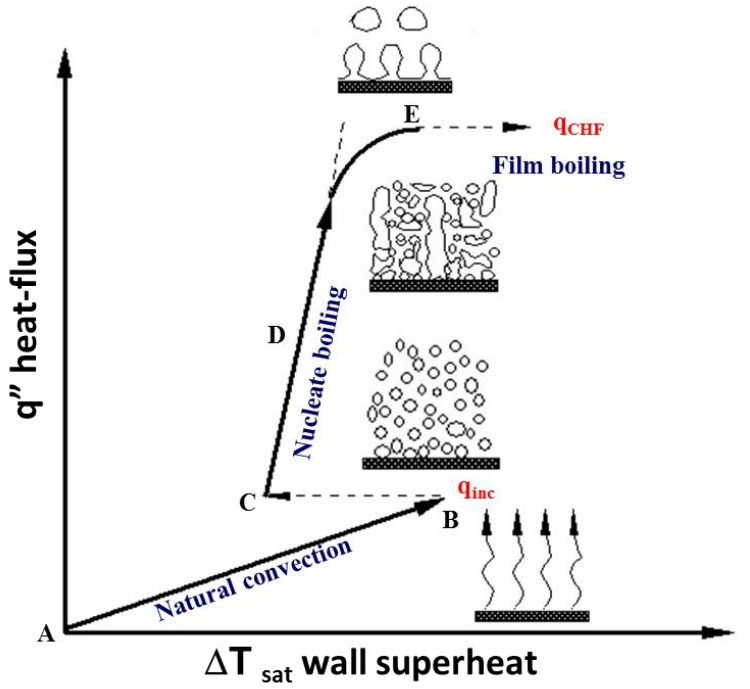

Figure 1.1 Characteristic pool boiling curve

There are generally three important parameters that should be considered when evaluating boiling heat transfer performance: incipient superheat, nucleate boiling efficiency, and CHF. Regardless of the application or fluid used, it is generally desirable to minimize the wall superheat required to initiate boiling to produce less thermal stress, to enhance the nucleate boiling heat transfer efficiency, and to increase CHF to give a larger heat flux operating range.

1.3.1 Incipience

Bubble initiates through heterogeneous nucleation for most boiling systems. Heterogeneous nucleation occurs at the interface between a liquid and the surfaces that contain it. This process is seeded by vapor or air trapped in the small cavities on the heated surface, as seen in Figure 1.2, which act as bubble embryos. Typically, this process requires only a few degrees of superheat before the onset of nucleation.

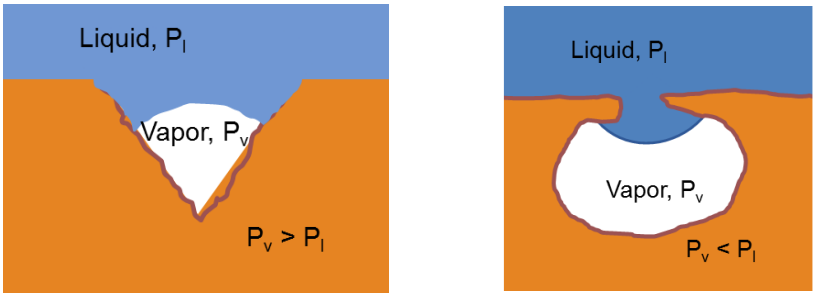

(a) Microcavity in plain surface (b) Re-entrant Cavity

Figure 1.2 Nucleation cavity

Incipience superheat required to initiate bubble growth from an embryonic bubble depends on the shape and size of the microcavity on the surface combined with the dynamic contact angle at the vapor/liquid/surface interface [9]. The microcavities on a plain surface are usually of the shape shown in Figure 1.2 (a), where the liquid-vapor interface is such that vapor pressure, P_v, is higher than liquid pressure, P_l. The pressure difference required for a bubble to grow can be estimated from equation (1-1). Smaller embryonic bubbles require larger superheats to initiate growth due to increased bubble vapor pressure.

$$P_v - P_l = \frac{2\sigma}{r_b} \tag{1-1}$$

However, for a cavity of shape as shown in Figure 1.2 (b), commonly referred as re-entrant cavity, the liquid-vapor interface curvature is reversed while entering the cavity through narrow opening, such that

vapor pressure is lower than liquid pressure [10]. In this case, it requires much less superheat to vaporize the liquid and grow the bubble. The growth of a bubble from a re-entrant cavity is shown in Figure 1.3. Such cavity is also able to increase the cavity volume without increasing the cavity opening so as to maximize the amount of gas/vapor entrapped by the wetting front [11]. Therefore, re-entrant cavities are ideal cavities for nucleate boiling process.

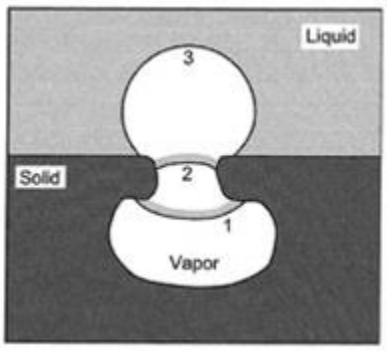

Figure 1.3 Growth of a bubble from a reentrant cavity [10]

Unfortunately, re-entrant cavities do not occur on the surface naturally. Therefore, many efforts have been made to artificially create such cavities in the form of mechanical structure or porous coatings to enhance nucleate boiling performance. Examples of such surface enhancement processes are discussed in chapter 1.4.

1.3.2 Nucleate Boiling

In pool boiling, the primary heat transfer mechanisms associated with nucleate boiling are latent heat transfer and microconvection. Latent heat transfer results from evaporation process when vapor bubbles grow in the superheated layer formed on the heated surface. Macro-evaporation occurs over the top of the bubble surrounded by the thermal boundary layer while micro-evaporation occurs underneath the bubble across the thin layer of liquid trapped between a rapidly growing bubble and the surface, referred to

as micro layer evaporation. Microconvection is caused by entrainment of the superheated liquid during bubble departure. Intense convection in the liquid adjacent to the heated wall is induced by the lateral pumping motion of growing and departing bubbles, which transforms the natural convection recess in to a localized forced convection process. In the other hand, Marangoni flow is another heat transfer mechanism that exist in nucleate boiling. It is caused by the surface tension gradient during the growth of the bubble. However, the contribution from Marangoni flow can be neglected for fully saturated condition.

Rohsenow [12] proposed one of the first nucleate pool boiling correlations, based on the bubble agitation mechanism (micro-convection). An empirical constant, C_{sf}, was introduced to account for the influence of the liquid-surface combination in his database. This correlation, equation (1-2), also points out the importance of the micro-topology of the boiling surface on nucleate boiling heat transfer.

$$\frac{q''}{\mu_l h_{lv}}\left[\frac{\sigma}{g(\rho_l-\rho_v)}\right]^{1/2}=\left[\frac{1}{C_{sf}}\right]^{1/r} Pr_l^{\,-s/r}\left[\frac{c_{p_l}(T_w-T_{sat}(P_l))}{h_{lv}}\right]^{1/r} \tag{1-2}$$

Mostinski [13] ignored surface effects while correlating heat transfer coefficients, α_{ab}, and formulated as a function of the reduced pressure of the fluid, p_r and its critical pressure p_{crit}. This correlation, equation (1-3), gives reasonable results for a wide range of fluids and reduced pressures.

$$\alpha_{nb}=0.00417\,q''^{0.7}p_{crit}^{0.69}(1.8\,p_r^{0.17}+4\,p_r^{1.2}+10\,p_r^{10}) \tag{1-3}$$

1.3.3 Critical Heat Flux

CHF occurs at the transition from the nucleate boiling regime to the film boiling regime. When CHF is reached, vapor film blankets the entire heating surface causing a rapid increase in surface temperature due to added thermal resistance of the vapor film. CHF is the limiting factor for most boiling systems

because achievement of CHF often leads to catastrophic failure by rapidly increasing surface temperature beyond the point where either the material melts or its structural strength is weakened.

While the exact mechanism of the cause of CHF is still not fully understood, many theories have been proposed to account for this phenomenon. Zuber [14] in his hydrodynamic instability model proposed that CHF occurrence is due to the instability of the vapor leaving the surface. He developed the following correlation to predict CHF under saturated pool boiling conditions:

$$q"_{cHF,z} = \frac{\pi}{24} h_{lv} \rho_v^{1/2} [g\sigma(\rho_l - \rho_v]^{1/4} \quad (1\text{-}4)$$

This correlation has been found to predict CHF well for plain surfaces, however, it doesn't take into account surface microstructure. His model has been later refined by Lienhard and Dhir [15] by including effect of surface geometry on CHF.

1.4 Boiling Heat Transfer Enhancement Methods

Various surface enhancement techniques have been explored to maximize boiling heat transfer performance for decades. Porous layer coatings have been the most effective technique so far to increase the boiling heat transfer coefficient and also to extend the critical heat flux. Porous layer coatings are composed of randomly arranged particles, often of varying sizes, producing pores and interconnecting channels providing flow paths for liquid supply and vapor escape. These coatings also create numerous micro-cavities that can trap vapors, which can be easily activated for the bubble nucleation process. Such cavities are usually referred as re-entrant cavities, depicted in figure 1.2. Bergles and Chyu [16] proved that the existence of reentrant cavities causes an increase in heat transfer because of stable and easily activated boiling sites. Thome [17] concluded that the primary enhancement mechanisms for re-entrant type enhanced surfaces were: enhanced nucleation from the larger embryonic bubbles, increased thin-film

evaporation due to the large internal surface area of the porous structure, and two-phase convection within the porous structure.

Porous layer coatings have evolved long way since Russian researchers like Malyshenko [18] utilized several millimeters thick meso-porous coatings to stabilize the boiling. The enhancement in boiling heat transfer was not significant because of large thermal resistance of the thick coatings and also use of non-conductive particles. High Flux [19] was the first commercially successful porous coating that showed promising results in boiling heat transfer improvement. These coatings were conductive, irregular shaped particles, brazed to the surface. The cavity size of the coatings had been reduced to fractions of a micron and the thickness to sub-millimeter scale. The initial application of High Flux was for air separation plants boiling liquid oxygen. Later, O'Neill, Gottzmann and Minton [20] compared the performance of four different fluids on a High Flux surface. They observed that the optimal porous structure depended on the fluid properties such as surface tension and thermal conductivity.

In addition to High Flux, numerous studies have been conducted on other types of porous coating materials. Various methods and techniques for constructing porous coatings were examined, including flame spraying (Almgren and Smith, [21]; Dyundin et al., [22]), electric sintering (Inoue, [23]), high current density electroplating (Albertson, [24]), electrogalvanizing (Trepp and Hooman, [25]). However, some of these coating procedures required extensive preparation and high equipment and operating costs, thus, often proved to be impractical and costly to implement in actual systems. Thus, their use either was limited to small scales or was simply abandoned.

O'Connor and You [1] introduced the concept of extra thin porous-layer coatings having layer thicknesses that are less than the superheated liquid layer thickness, referred as micro-porous coatings. The difference between a micro-porous coating and a conventional porous-layer coating is depicted schematically in figure 2. For conventional porous layer coatings, only the lower portion of the coating layer is activated during nucleate boiling, whereas, for micro-porous coatings, the entire coating layer is activated.

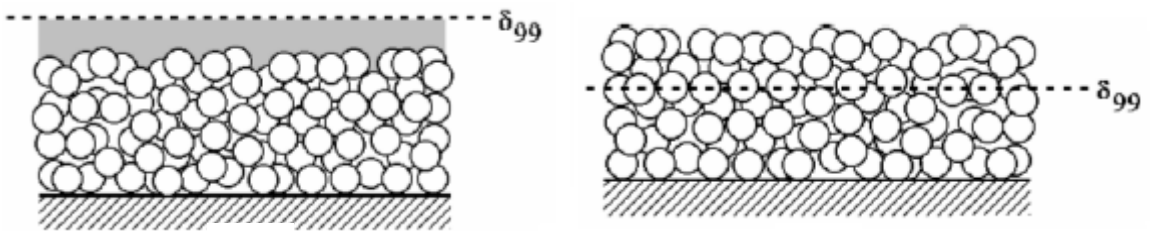

Figure 1.4 Schematics of (a) microporous coating and (b) Conventional porous-layer coating [1]

A benign method of applying micro-porous coating to the surface was developed and patented by You and O'Connor [1] which involved painting a mixture of silver flakes consisting of particles of diameters varying 3 to 10 μm, a binder (OB101 epoxy) and a carrier (Isopropanol) to the heated surface. The paint was cured under a lamp at 80 ^{o}C for about 2 hours. During curing, the alcohol evaporated and the mixture of flakes and epoxy adhered to the surface forming a micro-porous coating. The micro-porous coating produced by this benign (low temperature), economical technique was found to enhance pool boiling in saturated FC-72 with ~ 80% reduction in nucleate boiling superheat and a ~109% increase in the CHF limit over the non-painted surface.

Chang and You [26] later developed similar coatings using aluminum particles (1-20 μm) and copper particles (1-50 μm) along with Devcon Brushable-Ceramic epoxy as the binder and methyl-ethyl-ketone (MEK) as the carrier. Both aluminum (ABM) and copper (CBM) micro-porous coatings demonstrated significant enhancements of as much as ~ 109% increase in CHF, ~ 330% increase in nucleate boiling heat transfer and ~ 80% reduction incipience superheat relative to uncoated surface. ABM was subsequently used by Rainy and You [2] in pool and flow boiling heat transfer enhancement in flat and finned surfaces. Kim et al [3] also used ABM to study the effect of particle size in FC-72, R-123 and water and showed that optimum particle size exists for fluids with different surface tensions. Unlike in FC-72 and R-123, however, the boiling heat transfer was merely improved in water from ABM coated surface. This was because ABM utilizes smaller particle sizes which are not big enough to create larger cavities that are suitable for nucleation of water that has higher surface tension than refrigerants.

Other coatings of size scale similar to ABM have been studied since the invention of ABM by You and O'Connor [1]. Hwang and Kaviany [27] fabricated several copper micro-porous coatings by brazing the copper particles, and tested them in pool boiling of n-pentane. Most recently, 3M commercialized a boiling enhancement coating (BEC) [8] which is silver coated copper particles sintered to the surface. Thiagarajan et al. [28] showed excellent boiling performance of BEC in pool boiling as well as spray cooling of saturated HFE-7100.

Most of the coatings discussed above including ABM and sintered copper coatings have been assessed for only highly wetting fluids like refrigerants. Even though use of such fluids is common in electronics cooling industries, they are limited to low heat flux (<50 W/cm^2) applications. So water or water based fluids (water-glycol mixture) are often the choice of fluid for applications involving higher heat fluxes. Very few micro-porous coatings have been designed for boiling heat transfer enhancement of water. One of them is a sintered isotropic copper wire screens by Li and Peterson [7], however, sintering process itself involves costly equipment and high operation cost. Kim et al [3] introduced another thermally conductive micro-porous coating with the same simplicity and cost-effective fabrication approach as ABM, called TCMC. This coating was fabricated by soldering copper particles to the surface. To date, TCMC has shown the highest enhancement of nucleate boiling heat transfer in water. Despite of its good performance in water, it is limited to operating temperature which cannot exceed melting temperature of the solder paste (~200 ^oC) and also the potential corrosion due to galvanic potential difference between tin component of solder and copper. Therefore, in this study, the development of high temperature thermally conductive microporous coatings, Cu-HTCMC and Al-HTCMC, are conducted to upgrade the performance and reliability of ABM and TCMC, while maintaining the similar fabrication technique. Each coating is optimized for its composition, thickness and particle size to achieve the best possible combination of these parameters for pool boiling heat transfer of water.

CHAPTER 2

EXPERIMENTAL SETUP AND PROCEDURES

In this chapter, the various test sections and test heaters used in this study are described and the experimental procedures are explained. A total of three different test sections were designed and fabricated to carry out various experiments. The three test sections include pool boiling, spray cooling and jet impingement cooling test facilities. In addition, an uncertainty analysis is provided.

2.1 Test Heaters

Two different test heater surfaces were used in this investigation. They were copper and aluminum. Both types of heaters were fabricated almost identically except that for aluminum test heaters, bottom side of aluminum was nickel plated before soldering to the 20 Ohm resistor. Test heaters used in all three experiments, pool boiling, spray and jet-impingement tests, were essentially the same.

2.1.1 Copper Test Heater

As shown in Figure 2.1, a copper test heater is fabricated using a copper block (1 cm x 1 cm x 0.3 cm), a 1 cm x 1 cm heating element (20 Ω resistor; Component General Co.) a Lexan substrate, epoxy (420 DP; 3M) and wires. The copper block has one 1 mm diameter, 5 mm deep hole at 1.5 mm below the top surface for mounting a thermocouple. The heating element was soldered to the copper block and at the same time, a type-T thermocouple was embedded by soldering into the center of copper block through the hole described above. Two copper wires were attached to bus bars of the heating element to provide power to the heater. The assembly of heating element and copper block including wires was mounted on the Lexan substrate, copper side up. Then, epoxy was spread over the Lexan substrate, around the perimeter of the copper block, except for the top copper surface and was cured for 24 hours at room temperature.

The level of the epoxy was flush mounted with the top copper surface to prevent perimeter boiling during the boiling experiment. Both the epoxy and the substrate provided good insulation at the sides and the bottom. The heater surface temperature was later calculated from the temperature measured at the center of the copper block assuming 1-D steady state-conduction with k_{cu} ~401 W/m-K.

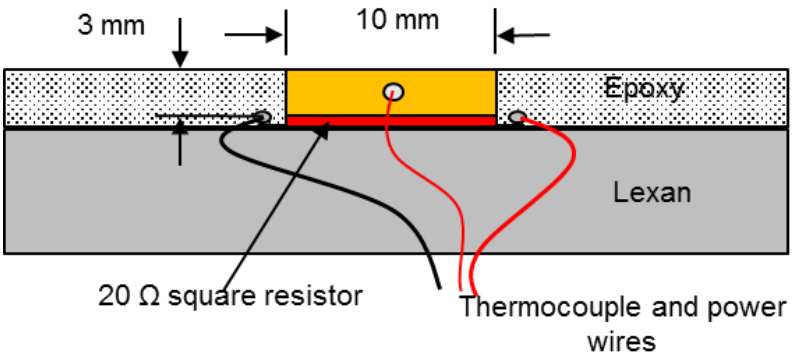

(a)

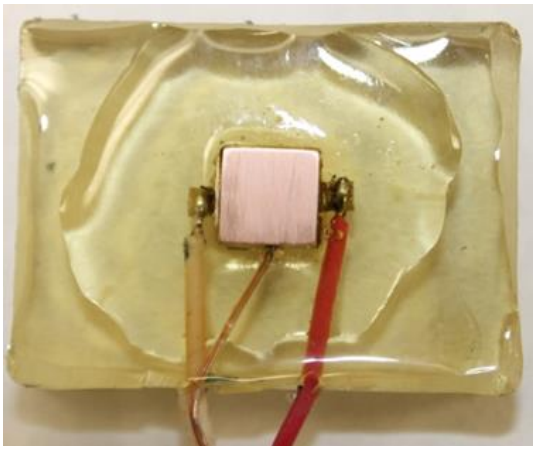

(b)

Figure 2.1 Copper test heater assembly (a) schematics and (b) picture

2.1.2 Aluminum Test Heater

Aluminum test heater was fabricated almost in the same fashion as copper test heater described in previous section. Only a minor change in fabrication method was required for aluminum test heater due to the inability to solder on the aluminum surface. For this reason, the bottom side of the aluminum (6061-T6) block (1 cm x 1 cm x 0.3 cm) was first plated with thin nickel layer, then soldered to the same heating element used for copper test heater. Instead of soldering thermocouple to the aluminum block, a thermally conductive epoxy (Duralco-R132) was used to secure the thermocouple inside the mounting hole. Before proceeding to use thermally conductive epoxy for thermocouple attachment in the aluminum test heater, this technique was validated on two copper test heaters, one using the thermally conductive epoxy, another using soldering for thermocouple attachment. The results of measured temperature (not shown) were identical which validated the use of thermally conductive epoxy to secure thermocouple in the aluminum test heater. Thermal conductivity of aluminum used for the heater surface temperature correction using 1-D steady-state thermal conduction was 237 W/m-K.

For boiling tests in acetone using aluminum heaters, a nylon substrate and R1442 epoxy (3M) were used instead of Lexan and DP 420 epoxy to insure compatibility with acetone. For the same reason, Teflon coated wires were used as power lead wires.

2.2 Data Acquisition System and Instrumentation

A computer controllable DC power supply (HP 6030A, 0-200 V, 0-17 A, 1000 W) was connected in series with the test heater and a shunt resistor (Crompton, Model 871-92UU-MTGB). The shunt resistor, rated at 100 mV and 10 A, was used to determine the current in the electric circuit. Even though the resistance of the heater was given by the manufacturer of the heater, current measurement using this nominal resistance would not be accurate as resistance constantly changes with temperature. Therefore, the use of shunt resistance minimized the error associated with current measurement. Eventually the heat

flux applied to the test heater was more accurately calculated from the product of current value calculated using the shunt resistance and its voltage drop, and the measured voltage drop across the test heater.

An HP 3852A Data Acquisition/Control Unit was used for all temperature, pressure and voltage measurements. An IBM compatible PC was used to control the data acquisition unit and power supply via an IEEE-4888 (GPIB) interface. A LabVIEW program was created and used to control the power supply and data acquisition unit during the tests.

2.3 Pool Boiling Test Setup and Procedures

This section describes the pool boiling test section and identifies its various components. It also discusses the procedures used to conduct pool boiling experiments.

2.3.1 Pool Boiling Setup

A schematic of the test vessel used for the pool boiling experiments is shown in Figure 2.2. The test chamber was made of anodized aluminum to ensure chemical compatibility with working fluid, especially acetone and also to reduce total weight. Gaskets and O-rings made of polypropylene were used also to ensure the chemical compatibility with acetone. The chamber had two reinforced glass windows on its front and rear sides as view ports. The external dimensions of the test chamber were 20 cm (wide) x 20 cm (length) x 17 cm (depth). Two half-inch diameter (1000 W) cartridge heaters were mounted near the bottom of the vessel to provide a rapid heating and stirring during the degassing process. Two silicon-rubber based band heaters were externally attached, one on each side of the vessel, and the power to those band heaters was controlled with an external temperature controller (PID) in order to maintain the steady saturation temperature of the bulk fluid. Two type-T thermocouples were placed within the test chamber to measure bulk liquid and vapor temperature. A pressure transducer, OMEGA PX202 (0-50 psia), was fitted though the top plate to measure the system pressure. An external, water-cooled condenser was

fitted to the top section of the chamber through a Swagelok valve in order to retrieve the condensed fluid back to the test chamber during the degassing process. Another Swagelok valve was used at the bottom of the test chamber for drainage after the experiments ended.

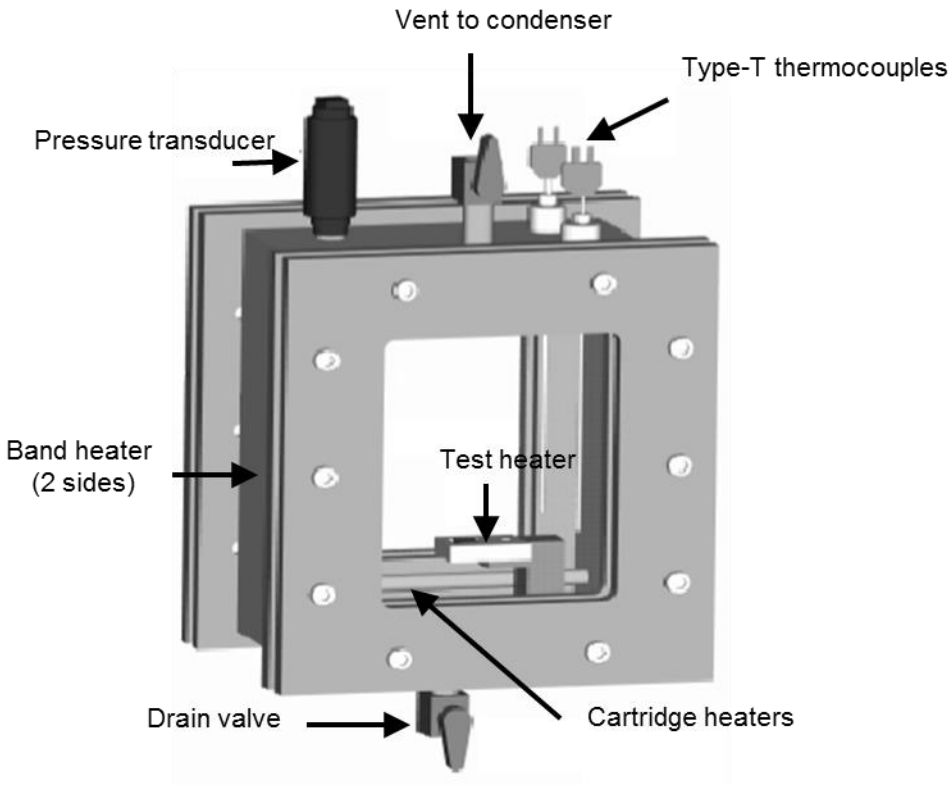

Figure 2.2 Pool boiling vessel

2.3.2 Pool Boiling Test Procedures

All boiling tests were performed with the test heater in the horizontal, upward facing orientation under increasing heat flux conditions. All tests were repeated to insure consistency and repeatability of the data. Distilled water is used as working fluid in the major portion of this study, however, other test fluids include acetone and HFE-7100. Selected thermal properties for each liquid are listed in Table 5.1. Prior to

all testing, the test chamber was heated to the test liquid's saturation temperature at atmospheric pressure using the band and the cartridge heaters. Once at its saturation temperature, the test liquid was boiled vigorously for at least 45 minutes with the top valve open to remove dissolved non-condensable gases from the test liquid. The condenser, located above the test section, allows any non-condensable gases to escape while simultaneously condensing any vapor back into the chamber to maintain the fluid level at 15 cm from the test surface. Then, the top valve was closed and cartridge heaters were turned off allowing only band heaters controlled by a PID temperature controller to maintain the saturation temperature. After the saturation temperature and the pressure were obtained and stabilized, testing began.

The power supply to the test heater and the data acquisition system were controlled by LabVIEW program. All the tests were performed in increasing heat flux condition till the CHF condition is reached. The temperature readings were taken once in every half a second for 50 seconds, the values were averaged, and the same process was repeated for the next 50 seconds. When the difference between consecutive average temperature values was less than 0.2 ^{o}C, steady-state was assumed, and the temperature readings and applied heat flux were recorded. Heat flux was then incremented to the next programmed level, and when steady state was reached, temperature readings and applied heat flux were again recorded. The program assumed that the CHF condition was reached when the heater temperature exceeded the previously recorded steady-state temperature by more than 20 ^{o}C. The power to the heater was then shut down and all the data including temperatures, pressure and heat flux were saved.

2.4 Spray Cooling Test Setup and Procedures

This section describes the spray cooling test section and identifies its various components. It also discusses the procedures used to conduct spray cooling experiments.

2.4.1 Spray Cooling Test Setup

A schematic of the spray cooling test setup is shown in Figure 2.3. A spray nozzle (IWATA airbrush) with nozzle diameter of 0.3 mm was firmly held by a metal stand and was connected to a compressed air source. For better control of the spray flow rate, a pressure regulator and air filter were used. The test heater was placed in vertical orientation facing the nozzle perpendicularly. In order for sprayed water to fully cover the heated surface, the distance between the spray nozzle and the heater surface was set to 1.5 cm, which was calculated using equation (2-1). The spray cone angle (θ) was measured to be ~38°.

$$H = \frac{L/2}{\tan(\frac{\theta}{2})} \tag{2-1}$$

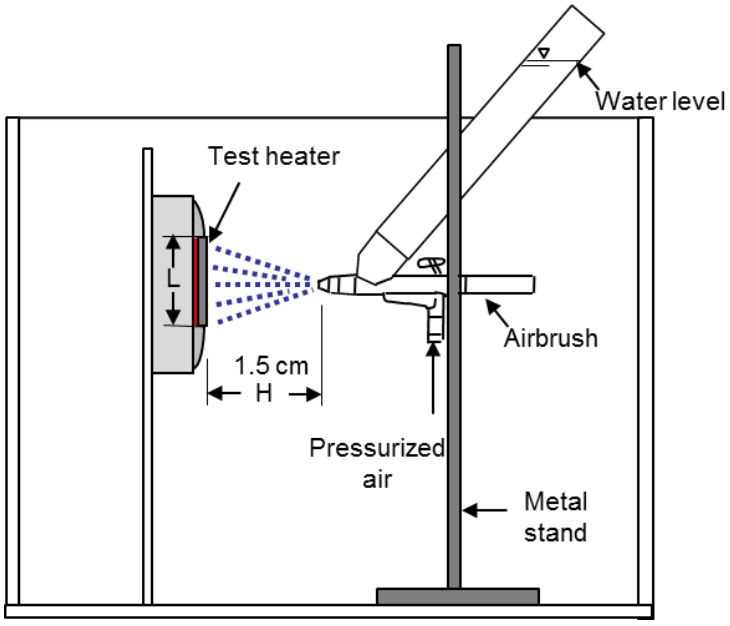

Figure 2.3 Spray cooling test setup

2.4.2 Spray Cooling Test Procedures

Spray cooling test was carried out in an open environment at room temperature. The flow rate was measured by dividing the total volume of water injected through the nozzle by the spray time. The flow rate was controlled by regulating the air pressure. Once the flow rate was fixed, power was applied to the test heater. When steady state was reached (in the same way as in pool boiling test), the heat flux was increased to next programmed level and this process was continued until CHF or the heater power limitation (250 W) was achieved. The CHF is assumed to be at the heat flux when the heater temperature exceeded the steady state heater temperature at previous heat flux level by 20 ^{o}C.

2.5 Jet-Impingement Cooling Test Setup and Procedures

This section describes the jet-impingement cooling test section and identifies its various components. It also discusses the procedures used to conduct jet-impingement cooling experiments.

2.5.1 Jet-impingement Cooling Test Setup

A schematic of the jet-impingement cooling test setup is shown in Figure 2.4. The setup consists of a stainless steel water reservoir with a pressure rating of 500 psig. It can hold up to 300 ml of water which is pressurized using compressed air. An Omega PX 302 pressure transducer, rated for 0 to 50 psia, is fitted to the top end of the reservoir to monitor the pressure inside the reservoir. Another end of the reservoir is connected to a solenoid valve through transparent Teflon tube. The solenoid valve is connected to a nozzle with internal and external diameters of 0.127 mm and 1.27 mm, respectively. The distance between the tip of the nozzle and heater surface was kept 1.5 mm (same as in spray cooling test) and the jet was centered at the heater surface.

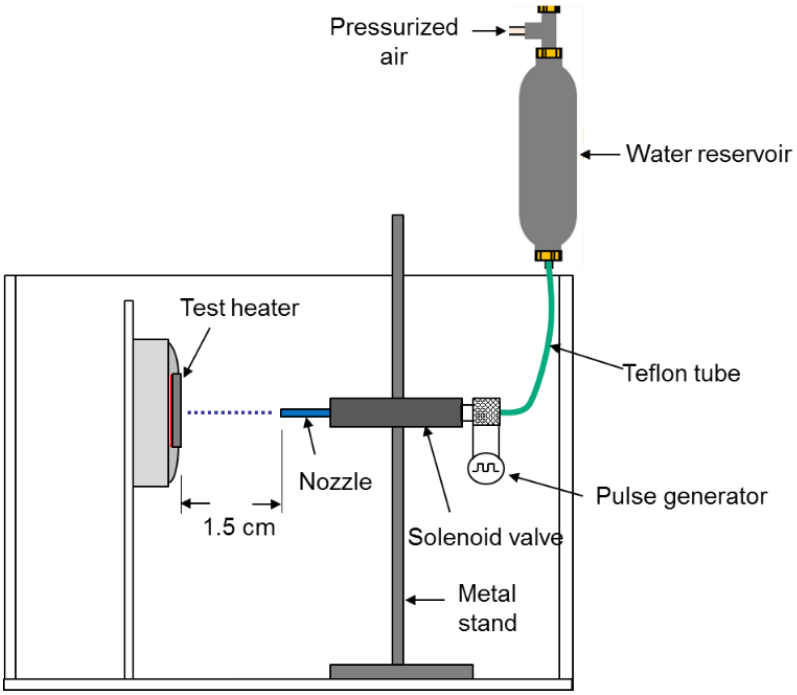

Figure 2.4 Jet-impingement cooling test setup

2.5.2 Jet-impingement Cooling Test Procedure

Jet-impingement cooling test was also done in an open environment at room temperature. Prior to the tests, the reservoir was filled with distilled water and pressurized using compressed air at 10 psi. Dispensing a discrete dose of droplets was made possible by a solenoid valve. It actuates upon receiving a signal from a pulse generator. A square pulse of 5 V was used with 800 ms pulse duration (PD) and 10 psi gage pressure to generate 56 nl droplet at 10 psi set pressure. The value of the droplet was calculated using microscope image and assuming the droplet is nearly spherical shape. The droplet volume depends on the PD and pressure applied, however, effect of droplet size was not the scope of this study, thus, not changed. The flow rate was changed by changing the frequency of signals at the pulse generator, which is determined by equation (2-2).

$$Q = f \times V_{droplet} \quad (2\text{-}2)$$

The flow rate, Q, was also reconfirmed by dividing the total volume of water injected through the nozzle by the dispensing time.

Initially water was dispensed at a certain frequency for ~1 minute before applying power to the heater in order to remove any trapped air inside the tubing between the nozzle and the solenoid valve. Then, the heat flux was increased with constant increments up to CHF. After each heat flux increment, the LabVIEW program was used to evaluate for steady state heater temperature before the next heat flux increment was made. Finally, the test was stopped when the CHF was reached.

2.6 Uncertainty Analysis

2.6.1 Heat Loss Estimation

A finite element analysis was conducted to estimate the heat loss through the insulation (sides and bottom) of a copper heater. A detailed 3-D model of a copper heater was created using SolidWorks which consists of all components of the actual heater (copper, resistor, lexan and epoxy) except power and thermocouple wires. Then the model was imported to ANSYS Workbench for the steady state thermal analysis. The heat transfer coefficients (*h*-values) and fluid temperatures, listed in

Table 2.1, were imposed on the heater FEM model and used to calculate the approximate heat loss through the heater insulation. These boundary conditions were chosen to obtain conservative estimates of the heat loss through the insulation during pool boiling of plain copper surface. The thermal conductivities of the components used are listed in Table 2.2.

Table 2.1 Imposed boundary conditions for the heat loss estimation

	h (W/m^2-K)	T_∞ (^oC)
10x10 mm heater surface	15000	100
All insulation surfaces (lexan and epoxy)	100	100

Table 2.2 Thermal conductivity used for the heat loss estimation

Materials	k (W/m-K)
Copper	400
Lexan	0.23
Epoxy	0.18

The FEM simulation results of the copper heater outputting 20 W are shown in Figure 2.5 FEM (ANSYS 15) temperature solutions for 10x10 mm copper heater: isometric view (left) and cross-section (right). The results revealed that the heat loss through the insulation at that heat flux (20 W/cm^2) is about 0.28 W or 1.4%. It should be noted that the FEM estimated heat loss was not deducted from any experimental data obtained.

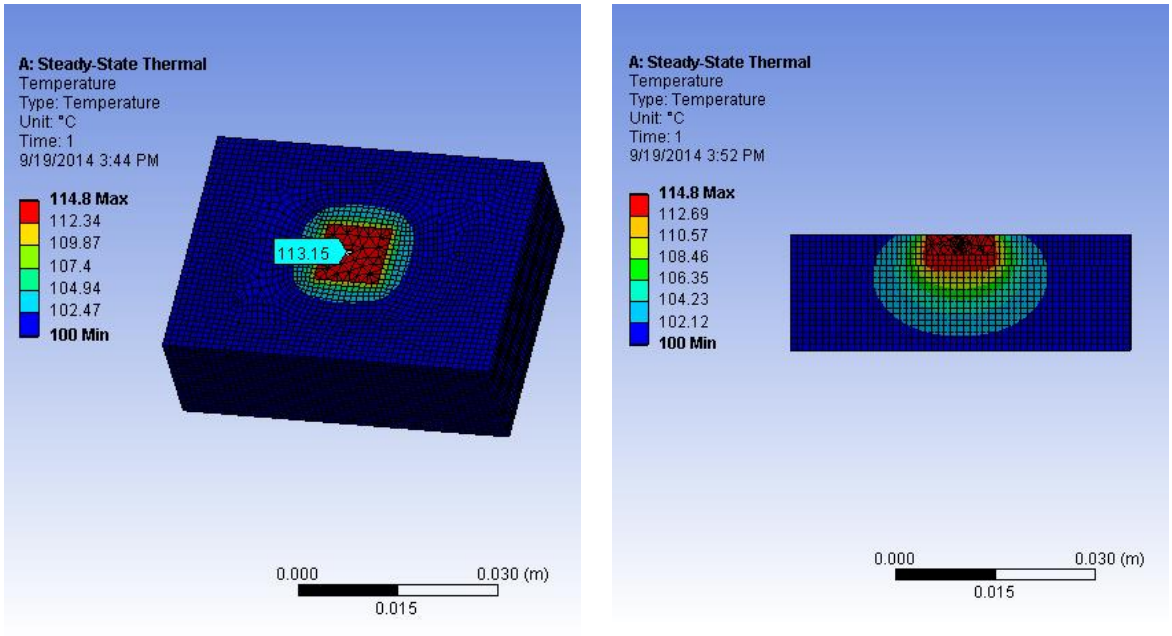

Figure 2.5 FEM (ANSYS 15) temperature solutions for 10x10 mm copper heater: isometric view (left) and cross-section (right)

2.6.2 Heat Flux Uncertainty Analysis

For all tests, heat flux was calculated using the 4-wire method. If the heater resistance is used to directly measure the current passing through the heater, and heat flux is calculated using that current, the calculated heat flux may have large error because the heater resistance may fluctuate with temperature. Instead, in the four-wire method, current passing through the heater is calculated by using known resistance of a shunt (R_s), connected with the heater in series, and voltage drop across the shunt (V_s). Then, by measuring the voltage drop across the heater (V_h) and the surface area of the heater (A_h), heat flux is given by equation (2-3).

$$q" = \frac{V_h V_s}{R_s A_h} \tag{2-3}$$

The uncertainty for the heat flux was estimated using the method of Kline and McClinktock [29]. By considering the errors due to voltage, surface area of the heater and the current applied, the heat flux uncertainty is given as equation (2-4).

$$\omega_{q"} = \sqrt{(\frac{\partial q"}{\partial V_h}\omega_{V_h})^2 + (\frac{\partial q"}{\partial V_s}\omega_{V_s})^2 + (\frac{\partial q"}{\partial R_s}\omega_{R_s})^2 + (\frac{\partial q"}{\partial A_h}\omega_{A_h})^2} \tag{2-4}$$

From the equation (2-4), the heat flux uncertainty was calculated to be ~5% at 100 W/cm^2 and the majority of which is due to the uncertainty of the resistance of the shunt resistor.

2.6.3 Temperature and Pressure Uncertainty Analysis

Temperature measurement uncertainty was estimated to be ±0.5 ^{o}C considering the thermocouple calibration error, temperature correction for the embedded thermocouples, and the thermocouple resolution error. In addition, the uncertainty in the pressure measurement was estimated to be less than 2.5%.

CHAPTER 3

MICROPOROUS COATINGS FABRICATION

This chapter will describe the fabrication techniques used for the development of copper and aluminum microporous coatings. These coatings were named HTCMC for High Temperature Thermally Conductive Microporous Coating. Most other porous coatings are destroyed at higher temperatures because the melting temperature of binding material is not sufficiently high. For this reason, copper and aluminum HTCMC are designed to withstand higher temperatures, up to 677 ^{o}C and 462 ^{o}C, respectively. Other significant advantages of these conductive coatings include improved conductivity because of the choice of metallic components, and lower risk of corrosion due to lower galvanic potential differences among components. In addition, the brazing technique used in the coating fabrication is easy and cost effective compared to other techniques that yield similar bonding strength such as plasma spraying and sintering processes.

3.1 Coating Components

3.1.1 Copper Microporous Coatings (Cu-HTCMC)

Copper microporous coating consists of copper powders, brazing paste (binder) and Isoparaffin. Copper powders are mostly spherical provided by Alfa-Aesar. Different particle sizes from 10 µm to 80 µm powders were used in this study. It was crucial that the copper powders not be oxidized otherwise the melted brazing alloy would have less wettability on the surface of copper powders while brazing. Brazing paste is composed of -325 mesh size (44 µm average size) Ag-Cu alloy that is suspended in a flux which removes the oxides at elevated temperature from the copper surface. Isoparaffin was used as a thinner to make a mixture of copper powders and brazing paste that could be painted on a flat surface. About 1.2 ml of Isoparaffin was used to mix 4.0 g of copper powders with different ratios of brazing paste. Slightly more

amount of Isoparaffin was added to the mixture in order to spread the mixture better to create thinner coatings. This slight change in the amount of Isoparaffin does not affect the end coating because the Isoparaffin is evaporated at the beginning of the brazing process.

3.1.2 Aluminum Microporous Coatings (Al-HTCMC)

Aluminum microporous coating consists of aluminum powders, brazing paste and Stoddard solvent. Spherical aluminum powders (Valimet, Inc.) from 10 μm to 110 μm sizes were used in this study. Brazing paste is composed of -200 mesh size Zn(78%)-Al(22%) alloy particles that are suspended in a flux. Stoddard solvent was used as a thinning agent for the mixture of aluminum powders and brazing paste that could be painted on a flat surface. About 1.1 ml of solvent was used for mixing 1.0 g of aluminum powder with different ratios of brazing paste. The amount of solvent was increased slightly to create thinner coatings.

The metal powders and brazing paste with the thinner were thoroughly mixed. Then, a small amount of mixture was dripped on the heater surface and spread uniformly by shaking and dripping excess amount out of the surface. Then the metal block was transferred to an oven for brazing.

3.2 Brazing Process

Brazing is a group of joining processes of metals by heating them to the brazing temperature that contain a filler metal having a liquidus above 450 ^{o}C and below the solidus of the base metals. The liquidus points for the filler metal alloys used in Cu-HTCMC and Al-HTCMC were 677 ^{o}C and 462 ^{o}C, respectively. However, in order to make sure all filler metal particles melt and reflow, a maximum brazing temperature of 20 ^{o}C above the liquidus point was recommended by the manufacturer.

The brazing process was carried out in a Carbolite, Ltd. tube furnace (maximum temperature of 1200 ^{o}C) in a reduced oxygen environment. Industrial grade Nitrogen gas was pumped into the oven approximately for two minutes prior to heating the oven and maintained throughout the entire brazing process. This allowed the air inside the oven to be low of oxygen content. Such reduced oxygen environment was important because the oxidation of the metal powders and the substrate surface interferes with the wetting and flow of the melted brazing alloy.

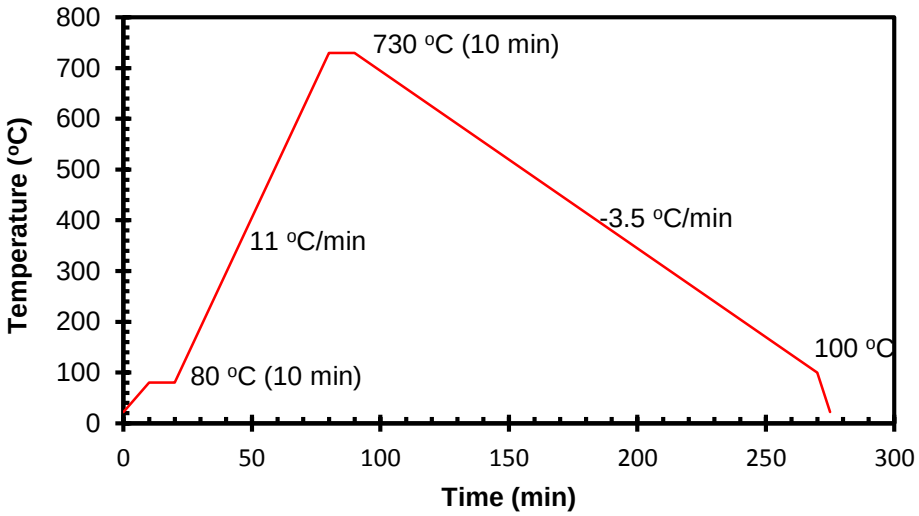

Figure 3.1 Thermal cycle used for brazing process of Cu-HTCMC

Figure 3.1 shows the thermal cycle used for brazing Cu-HTCMC. The only difference in this process for Al-HTCMC was that the maximum brazing temperature was set to be 530 ^{o}C instead of 730 ^{o}C. The oven was first ramped from room temperature to 80 ^{o}C and held for 10 minutes to allow the solvent to evaporate from the coating. If the solvent was not evaporated initially, the trapped solvent would explode through the coating paste at higher temperature and that would have created craters resulting into non uniform coating. After the 10 minute dwell time, the oven temperature was ramped from 80 ^{o}C to 730 ^{o}C for

Cu-HTCMC and to 530 ^{o}C for Al-HTCMC, where it was held for additional 10 minutes to allow the brazing alloys to melt and flow. It was necessary to heat the oven to more than 50 ^{o}C above the liquidus point of brazing alloy because the actual temperature of the substrate was mostly found to be lower than the oven's programmed temperature. This was partly due to the cooling effect from Nitrogen gas. Finally, the oven was turned off and the sample was left inside the oven to cool with continuous supply of Nitrogen gas in order to avoid oxidation.

3.3 Cleaning Process

Even though flux is an integral component of the brazing paste for its reflow, the flux residue left in the coating after the brazing process can cause several issues if not removed. This residue not only clogs the pores, but also makes the coating unstable for the boiling test. In addition, due to presence of highly reactive element such as Fluoride in the residue, the flux may be a factor for severe corrosion in the long run. Therefore, it is very important to carefully clean the coating after the brazing process.

Cu-HTCMC was cleaned using 5% acetic acid in an ultrasonic bath (42 Hz) at 40 ^{o}C bath (water) temperature for 5 minutes. Acetic acid at 5% concentration is known to have very little etching effect to the copper, yet it was very effective on removing the flux including oxides. The coating was further cleaned using distilled water for 5 minutes, then using acetone for another 5 minutes in ultrasonic bath at room temperature. Finally, the coating was rinsed with distilled water and was air dried. Similarly, Al-HTCMC was cleaned in the same setup using 5% alkali solution for 10 minutes, then distilled water for 5 minutes, and then acetone for 5 minutes. Lastly, the coating was rinsed with distilled water and air dried.

Besides flux residue, some of the loose metal powders would detach during ultrasonic cleaning. This was used as a measure of bonding strength. If less than approximately 5% of particles detached from the surface, the coating was considered to have satisfactory bonding strength. This also assured that there would be no contamination due to particle detachment from the coating during testing or other operation.

3.4 Powder Size Distribution

Even though the metal powder manufacturer stated an average particle size, this was based on the probability from a mesh. Therefore, the average particle size (APS) of each powder was determined by taking SEM photos and measuring diameter of 500 particles. APS is the mean value of those diameter measurements. Particle size distribution for both copper and aluminum is shown in Figure 3.2 and Table 3.1, which indicate that larger the mean powder size, the larger the size distribution is.

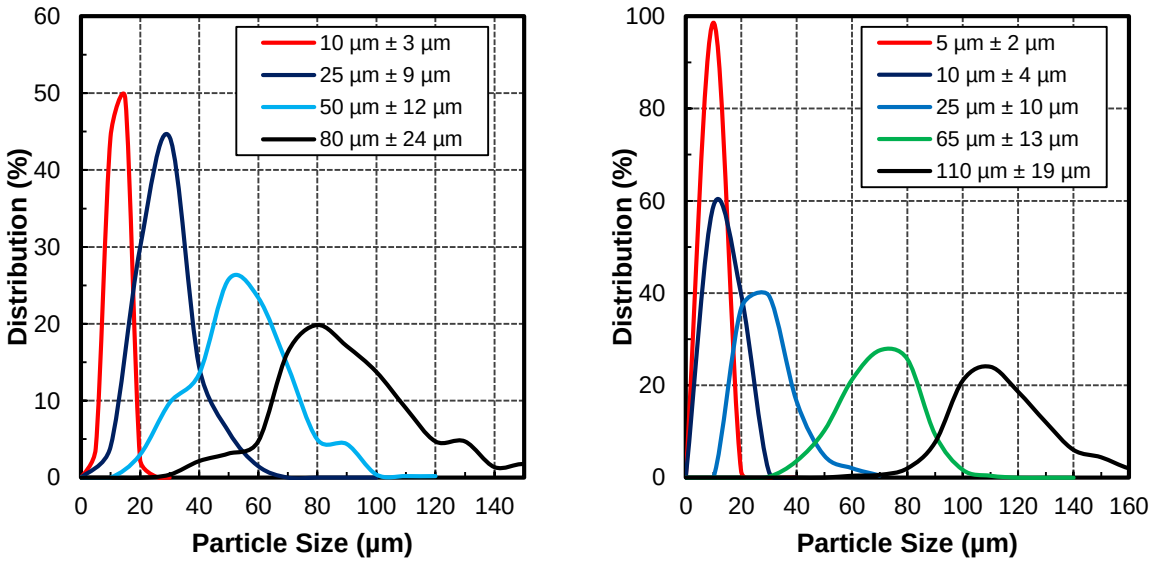

Figure 3.2 Particle size distribution of copper (left) and aluminum (right)

Table 3.1 Particle size distribution (μm)

	APS	Mean	St. Dev.	Min.	Max.
Copper	10	10.05	2.53	2.66	21.14
	25	24.46	9.34	4.64	59.83
	50	49.66	16.45	11.54	114.35
	85	84.65	23.69	23.79	162.68
Aluminum	5	5.22	2.06	1.60	15.76
	10	9.64	4.33	2.80	22.59
	25	25.04	10.08	10.19	63.39
	65	64.70	13.16	28.16	101.08
	110	109.87	18.90	52.47	171.23

CHAPTER 4

POOL BOILING RESULTS

4.1 Plain Surface for Reference

4.1.1 Plain Copper

Experiments were first conducted using plain copper surface such that its pool boiling characteristics can be used as reference to compare with microporous coated surfaces and to qualify the test loop by comparing with existing accepted correlations. The plain copper surface used in this study was polished using 600 grit sand paper and its roughness was measured to be 0.1 µm.

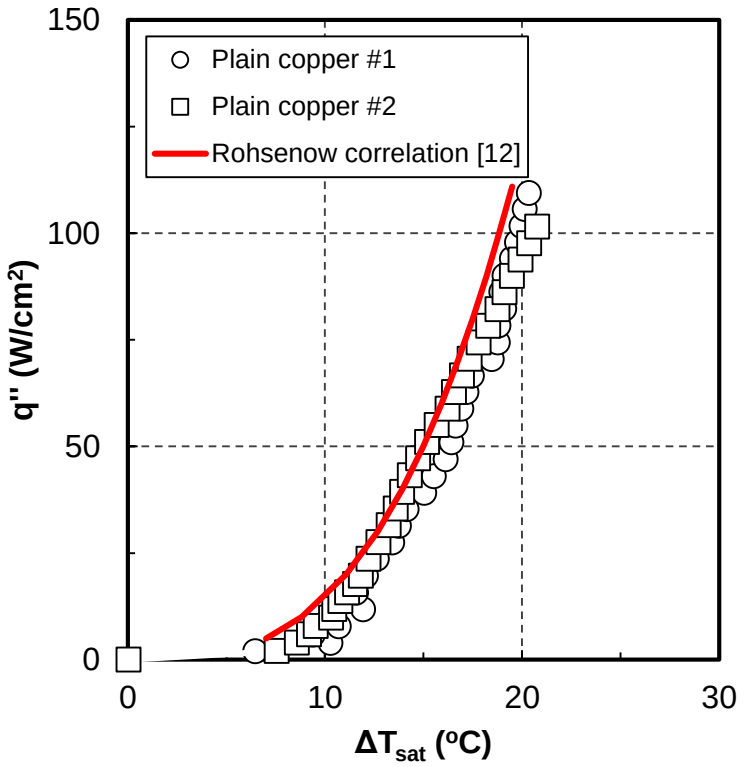

Figure 4.1 Reference pool boiling curve from plain copper surface

Two sets of pool boiling curves from two separate plain copper heaters are shown in Figure 4.1. The last data point at the end of the boiling curves, in this figure or in all future figures, indicates the onset of CHF. As illustrated, the boiling heat transfer coefficients data obtained in the current investigation are in very good agreement with Rohsenow correlation [12], and the CHF data are also very close to that predicted from Zuber's correlation [14]. These results confirm that the current facility can be used to provide highly repeatable data.

4.1.2 Plain Aluminum

A plain aluminum surface, polished on a 600 grit paper was used to generate a reference pool boiling curve to compare with aluminum microporous coatings. Roughness of plain aluminum surface was measured to be 0.3 μm, much higher than plain copper surface, even though both surfaces were polished on the same grit paper with the same technique. This difference in surface roughness could be due to the different hardness of copper and aluminum.

Figure 4.2 shows repeated pool boiling test results of plain aluminum surface in water for the reference curve. The results couldn't be compared with Rohsenow correlation as surface-liquid property (C_s), used in the correlation, is not available for aluminum-water. There are no pool boiling results reported for plain aluminum surface with flat geometry and for the same size as in this study to compare with the current results. The results indicate that plain aluminum surface has unusually high CHF compared to that of plain copper surface and this is attributed to increased wettability of water due to oxidation of aluminum surface during boiling. Aluminum has high proclivity to form aluminum oxide even in contact with air. Oxidation of aluminum in water is more rapid and is accelerated at high temperature forming aluminum hydroxides and oxides. Because of such formation of oxides layer, the wettability of the surface increases. Contact angle measurement on aluminum surface before and after the boiling tests shows the dramatic reduction in contact angle from 70^o to less than 20^o. As the wettability increases, CHF increases, since

liquid can quickly rewet the local dryout locations at high heat flux. This relationship between wettability and CHF is reported by multiple researchers [30] [31] [32].

Oxidation is usually a transient process, which may result into transient nucleate boiling results. However, results of repeated boiling tests in Figure 4.2 show non-transient characteristics. There was insignificant change in nucleate boiling heat transfer results when the boiling tests were repeated three times. This is because the surface was most likely oxidized during the degassing process and there was minimal additional oxidation during the actual boiling test.

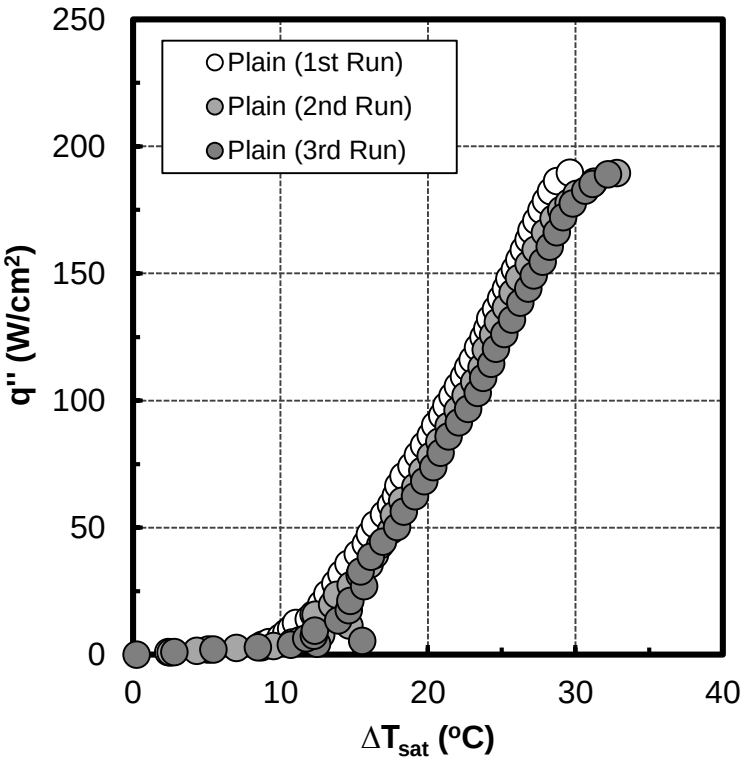

Figure 4.2 Reference curve for plain aluminum surface

4.2 Stability of the coating

As previously stated, surface energy on the microporous surface can be affected by factors such as oxidation and aging that can result into transient boiling results. In order to validate the steady state results from pool boiling tests of Cu-HTCMC and Al-HTCMC, tests were repeated over the same coated surface. Figure 4.3 shows the results of 50 µm particle size Cu-HTCMC tested four times and of 85 µm particle size Cu-HTCMC tested two times consecutively. Similarly, Figure 4.4 shows the results of 25 µm particle size Al-HTCMC tested three times consecutively. For all Cu-HTCMC and Al-HTCMC coatings, repeated boiling curves overlap denoting no change in boiling heat transfer due to oxidation or aging during the pool boiling tests. This validates the comparison between the boiling curves from one test to another obtained over the coated surfaces.

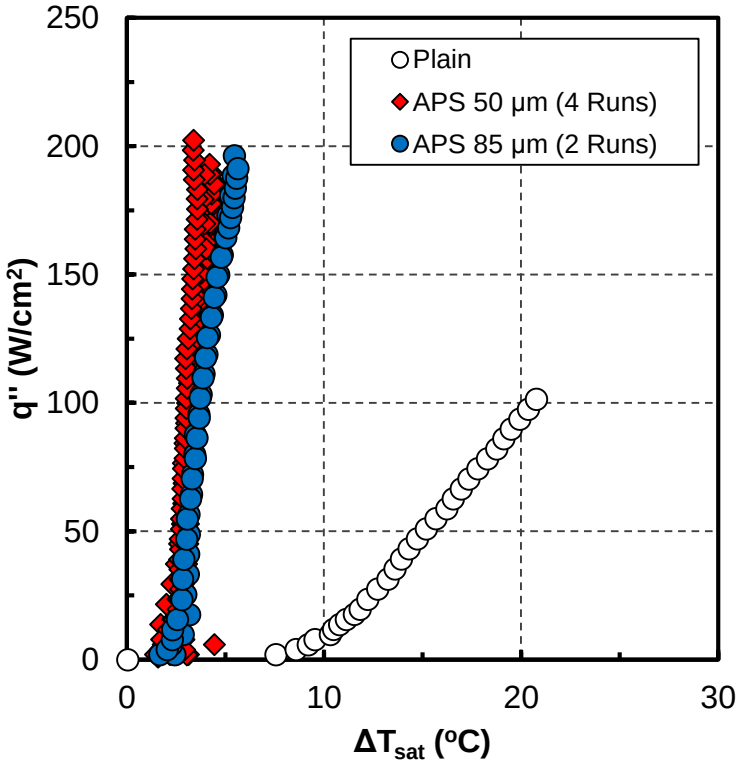

Figure 4.3 Pool boiling curves of repeated tests on Cu-HTCMC coatings

More importantly, it is notable that the heat transfer coefficient is significantly improved by both Cu-HTCMC and Al-HTCMC compared to the plain surface. As discussed in the introduction, microporous coatings facilitate increased number of nucleation sites during boiling. For example, Figure 4.5 shows more nucleating bubbles arising from the coated (Cu-HTCMC) surface compared to plain copper surface at the same heat flux of 5 W/cm^2. The bubble departure frequency was also much higher in the case of coated surface compared to plain surface. These phenomena are well described in literatures [33].

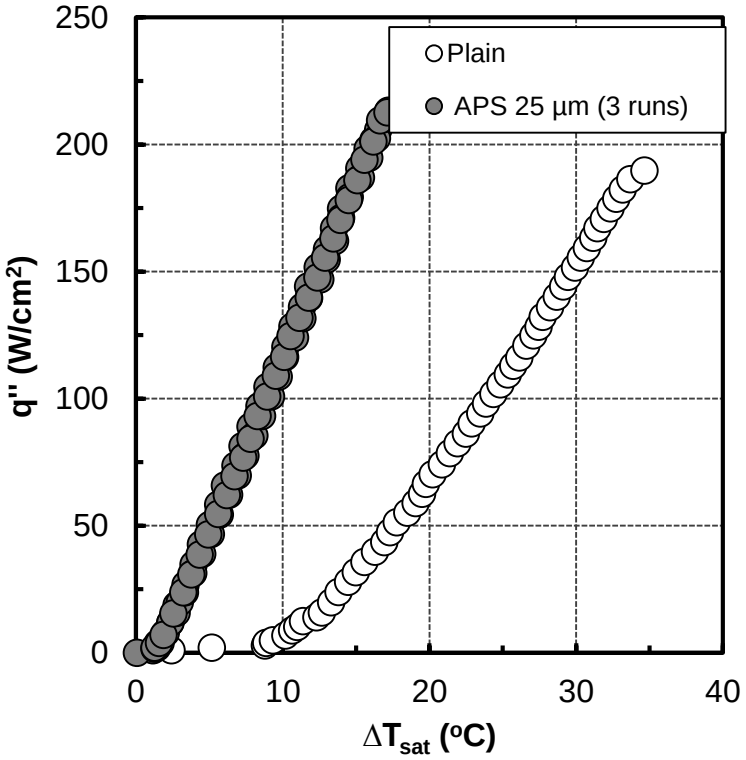

Figure 4.4 Pool boiling curves of repeated tests on Al-HTCMC coatings

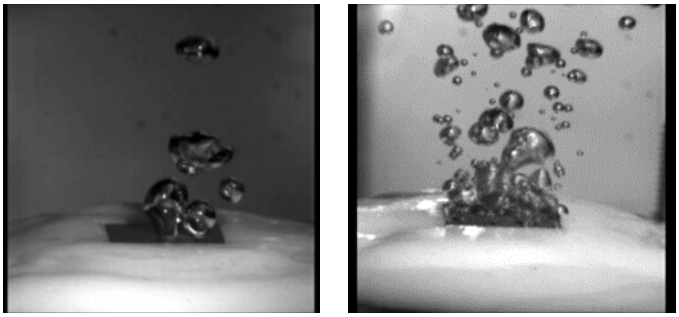

Plain copper Cu-HTCMC

Figure 4.5 Images of boiling on plain and Cu-HTCMC surfaces at 5 W/cm^2

4.3 Coating Optimization

There are three parameters which control the porosity and therefore, number of nucleation sites in a microporous coating formed by metal powders and a binder. Those parameters are mass ratio of metal powders to binder (mixing ratio), coating thickness and particle size. In order to achieve best nucleate boiling heat transfer, coating optimization was performed with these three parameters. Although these parameters are dependent on each other, the effort was to find the best possible combination of these parameters.

4.3.1 Effect of Mixing Ratio (Composition)

The mixing ratio is defined as the ratio of mass of metal powders to the binder used in manufacturing the coating. As seen in previous investigations by You et al [34] and Kim [3], this ratio can have large effect on the performance of the coating. The mixing ratio is inversely proportional to the amount of binder in the coating. That means increasing mixing ratio refers to decreasing amount of binder in the coating. The schematics in Figure 4.6 explain the effect of mixing ratio on porosity of the coating. For higher mixing ratios, there may not be enough binding material to bond the coating particles with each other and with the substrate which may result in uncoated space on the substrate. On the other hand, for lower mixing

ratios, binder can clog the pores eliminating the potential nucleation sites. In addition, excess binder can settle on the bottom of the substrate adding thermal resistance. Therefore, the ratio can affect the coating's bonding strength, its porosity and pore size. In turn porosity and pore size affect the nucleation site density, consequently, the boiling performance.

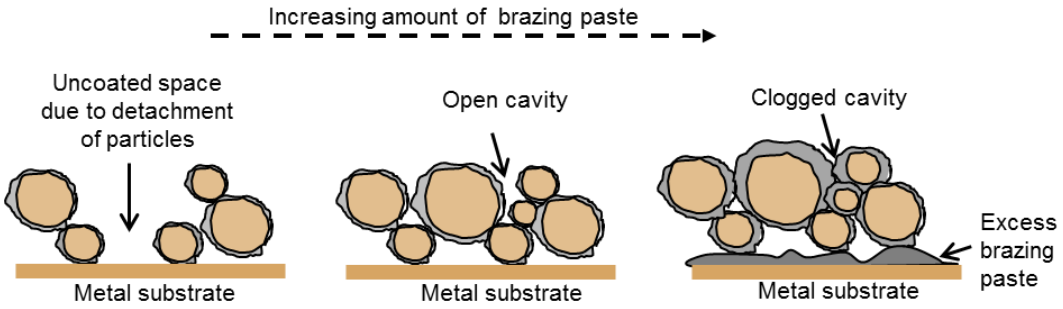

Figure 4.6 Schematic showing the effect of brazing paste amount on porosity

4.3.1.1 Cu-HTCMC

During the development of TCMC by Kim [3], it was found that TCMC had an optimized mixing ratio of 2.0:1.0. The initial mixing ratio of Cu-HTCMC was based near this value. Five different mixing ratios 1.8:1.0, 2.2:1.0, 2.8:1.0, 4.0:1.0, and 5.0:1.0 were tested and their SEM images (top view) are shown in Figure 4.7 (a). The coatings were made from 50 μm particles while keeping the coating thickness approximately the same (~165 μm). As the figure indicates, with the increasing amount of binder/brazing paste, the cavities or pores are narrower because of the clogging effect. The same trend can be clearly observed from cross-section of the coatings, listed in Figure 4.7 (b).

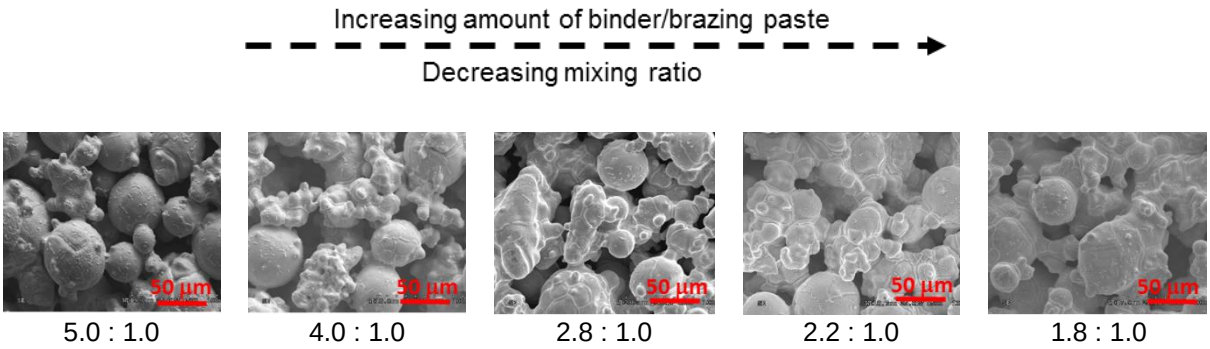

(a)

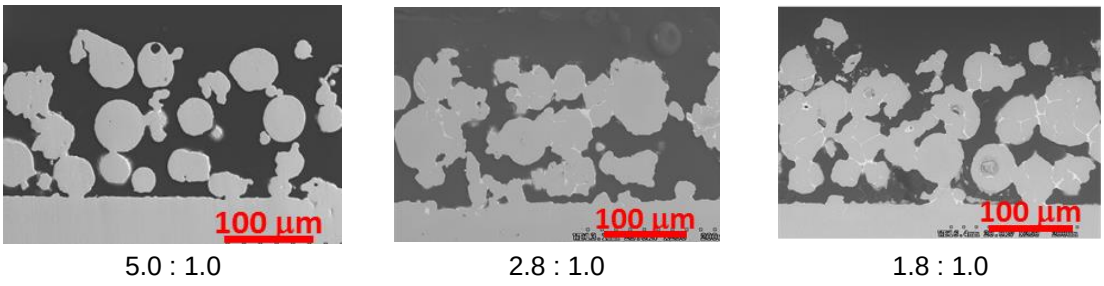

(b)

Figure 4.7 SEM images of Cu-HTCMC with different mixing ratios: (a) top view (b) cross-section

The clogging of the pores can also be validated from the porosity measurement of the coatings, shown in Figure 4.8. The porosity is defined as the ratio of porous volume to the volume of particles and pores combined. This was measured from the cross section of each coating such as Figure 4.7 (b) using image processing technique. The detail method is given in APPENDIX A. As shown in the figure, the porosity is continuously reducing as the mixing ratio decreases.

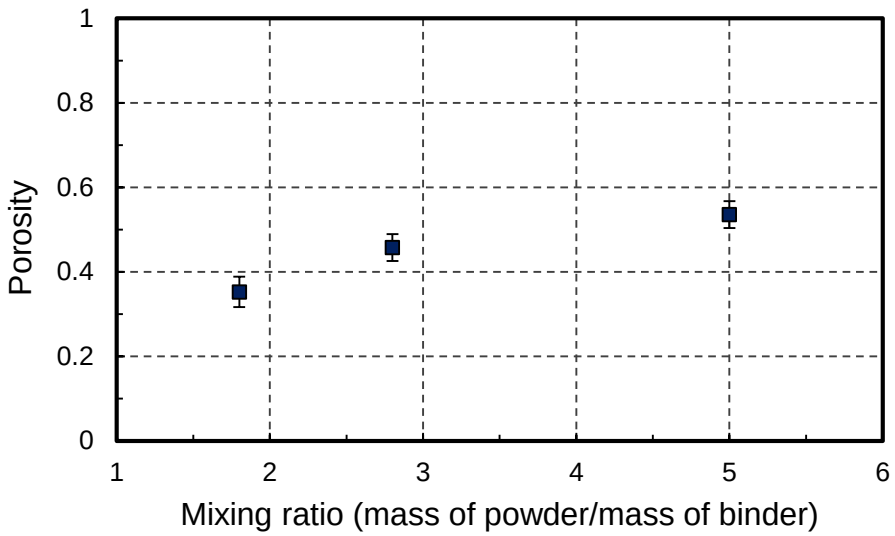

Figure 4.8 Effect of mixing ratio on porosity of Cu-HTCMC

Figure 4.9 illustrates the pool boiling results of Cu-HTCMC with various mixing ratios. As the figure shows, pool boiling heat transfer rate increases with the increase in mixing ratio up to 2.8:1.0, then decreases with further increasing the ratio. The increase in heat transfer rate with the increasing ratio can be attributed to increase in porosity and increased number of nucleation sites, since less number of pores are clogged with less amount of brazing paste present. However, the degradation of the heat transfer by increasing ratio beyond 2.8:1 might be due to the larger pore openings (less re-entrant type cavities) formed in the coating (Figure 4.7 (a) and (b)), that allow the liquid to flood the cavities by the liquid and minimize the gas entrapment which is important for nucleation activation. But, this effect can ease the liquid replenishment to dry spots at higher heat flux compared to the case where pores are clogged. This could be the reason why CHF seemed to increase as the mixing ratio was increased, as shown in the Figure 4.9. With this result, 2.8:1 ratio was determined as optimum mixing ratio for Cu-HTCMC and kept the same ratio for the study of other parameters (thickness and particle size).

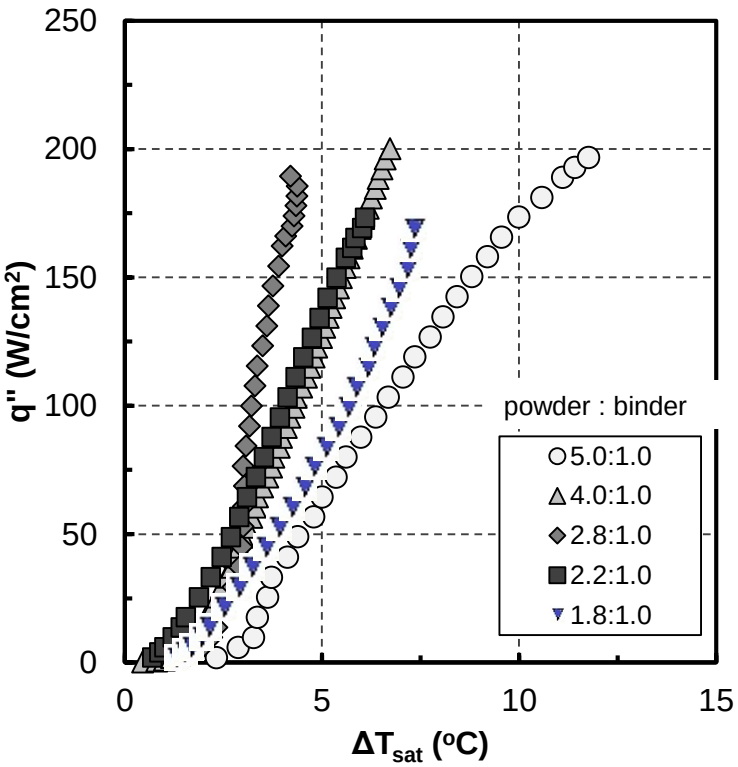

Figure 4.9 Effect of mixing ratio on the pool boiling performance of Cu-HTCMC

4.3.1.2 Al-HTCMC

In the case of Al-HTCMC, the weight of the particles content and the volumetric Stoddard solvent content were fixed at 1.0 g and 1.2 ml, respectively. With a fixed weight of particles and a fixed volume of Stoddard solvent, the weight of the binder was varied. Three different mixing ratios were tested, 1.4:1.0, 1.0:1.0 and 0.7:1.0.The mixing ratios are much smaller compared to those of Cu-HTCMC because of the density of aluminum being much less than that of copper. The coatings were made from 65 μm particles while keeping the thickness approximately same (~200 μm). The pool boiling results of Al-HTCMC with different mixing ratios are shown in Figure 4.10. As shown in the figure, mixing ratio of 1.0:1.0 resulted in maximum boiling heat transfer. The degradation of boiling heat transfer with less or more than this ratio could be again due to particle detachment or clogged pores. The effect of mixing ratio on CHF is also

consistent with that of Cu-HTCMC, i.e. as the mixing ratio increases, CHF also increases. More open pores at higher mixing ratios coatings are responsible for higher CHF as liquid can easily rewet the surface at high heat flux delaying CHF. For optimization of Al-HTCMC with respect to other parameters (thickness and particle size), 1.0:1.0 ratio was maintained.

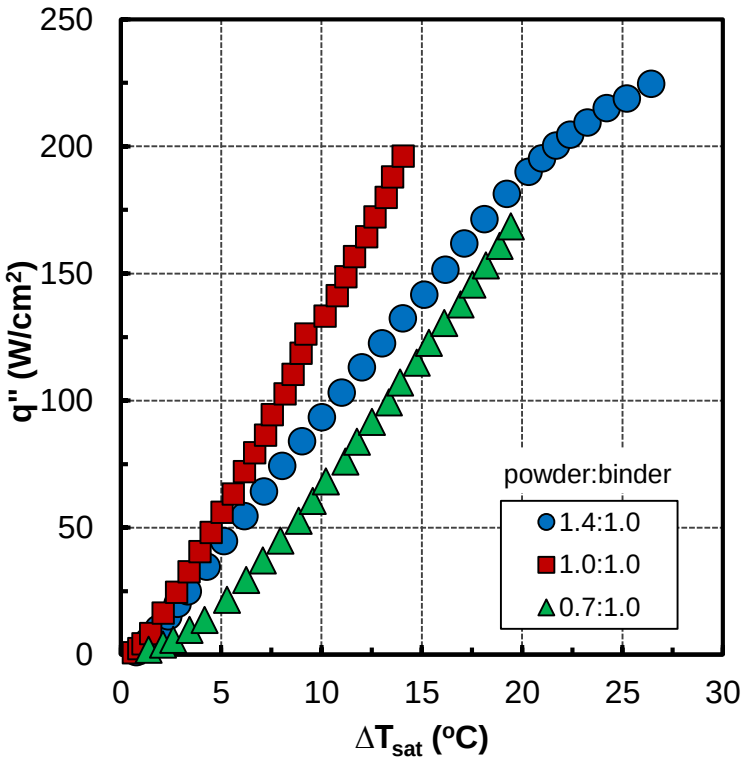

Figure 4.10 Pool boiling results of Al-HTCMC for different mixing ratios

4.3.2 Effect of Coating Thickness

Thickness plays an important role in the boiling performance of micro-porous coatings. The boiling performance usually degrades when thickness increases. The study by O'Connor and You [1] on the effect of microporous coating thickness is one of many examples reported. Such boiling degradation with increased thickness is believed to be due to added thermal resistance, increased liquid hydraulic resistance

and increased vapor removal resistance. Added thermal resistance from increased thickness is more prominent for the coatings whose effective thermal conductivity is relatively low, for example ABM. The increased hydraulic resistance impedes the liquid from quickly rewetting the inner most parts of the coating, while increased vapor removal resistance inhibits the vapor to escape from within the coatings. Hence, the thickness of the coating should be reduced to its lowest practical limit of the coating fabrication without minimizing the number of cavities.

4.3.2.1 Cu-HTCMC

O'Connor and You [1] reported that the thickness of the micro-porous coatings (ABM), for optimum boiling, depends on the average size of the powder. They concluded that the optimum thickness would be 5 times the average size of the powder. In the current study, three thicknesses were tested, 240 µm, 165 µm and 130 µm using 50 µm size particles. As shown in Figure 4.11, unlike in the case of ABM [1], a thickness approximately 5 times the average powder size (240 µm) resulted in the worse heat transfer performance. This could be due to the difference in powder size distributions used for ABM and Cu-HTCMC. Powders used in ABM coatings were much smaller and had a narrow range of size (1-20 µm) whereas the powders used in this study had wide range (12-114 µm) as indicated in Table 3.1. The thickness nearly 3 times the average powder size (165 µm) produced much higher heat transfer coefficient. However, the degradation of heat transfer for thicker coating is again attributed to added thermal and hydraulic resistances. On the other hand, the heat transfer coefficient for the coating of thickness less than 3 times the average powder size degraded significantly because as the thickness is reduced to less than 3 times the average powder size, the porosity increases but the number of reentrant type cavities are reduced. The effect of thickness on CHF is clearly shown in the Figure 4.11. As the thickness increases, the CHF also increases due to the fact that for thicker coatings, larger volume of liquid flow with in the porous coatings is available.

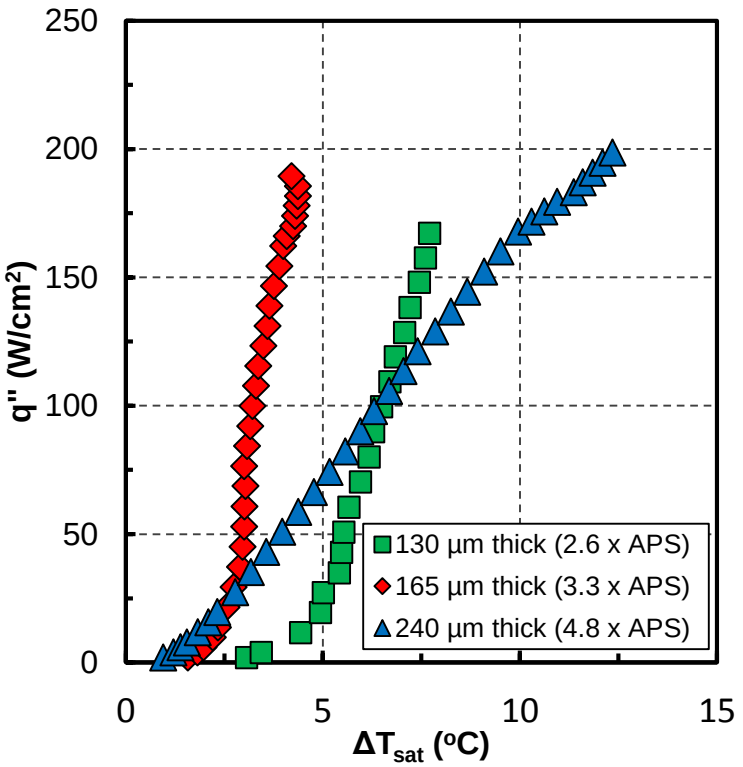

Figure 4.11 Effect of coating thickness on pool boiling performance of Cu-HTCMC

4.3.2.2 Al-HTCMC

For Al-HTCMC, thicknesses ranging from 170 µm to 370 µm were tested using 65 µm size particles. Figure 4.12 shows the difference in nucleate boiling heat transfer due to increase in thickness. Similar to Cu-HTCMC, Al-HTCMC with thickness to particle size ratio of ~ 3 (200 µm thick) resulted in the maximum boiling heat transfer. As expected, the boiling heat transfer degraded while CHF was improved as the thickness increased. Below 200 µm thickness, the boiling heat transfer was worsen due to less reentrant cavities as the thickness to particle size ratio becomes below 3.

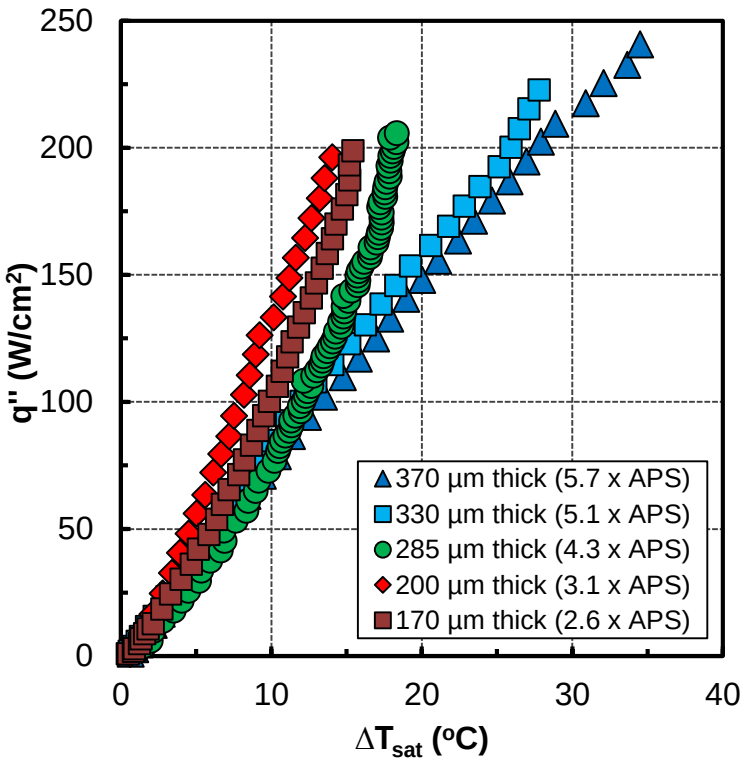

Figure 4.12 Effect of coating thickness on pool boiling performance of Al-HTCMC

4.3.3 Effect of Particle Size

The nucleation process is very much dependent on the size of the cavity in the coatings [10], which is directly proportional to the particle size. As the cavity size decreases the pressure required for bubble departure increases. Based on Equation (1-1), the amount of superheat required to initiate nucleate boiling depends on fluid properties (surface tension) and the bubble radius (cavity size). Equation (4-1), derived in [10], implies that for a given level of superheat, a cavity will be active if its radius is greater than a critical value r^*. Using this equation, the cavity diameter required to generate embryonic bubbles for superheats of 5 ^oC at 100 ^oC saturation temperature can be calculated to be ~6.5 µm. However, for the lower superheats, this value dramatically increases as shown in Figure 4.13. So, as the cavity size is larger, the superheat required for nucleation becomes lesser. However, when the cavity size is too big, then the bubble size may

become larger and the number of nucleation per unit area becomes less. Therefore, it can be concluded that there exists an optimum particle size for a given working fluid.

$$r^* = \frac{2\sigma T_{sat\ @\ P_l}\ v_{lv}}{h_{lv}[T_l - T_{sat\ @\ P_l}]} \tag{4-1}$$

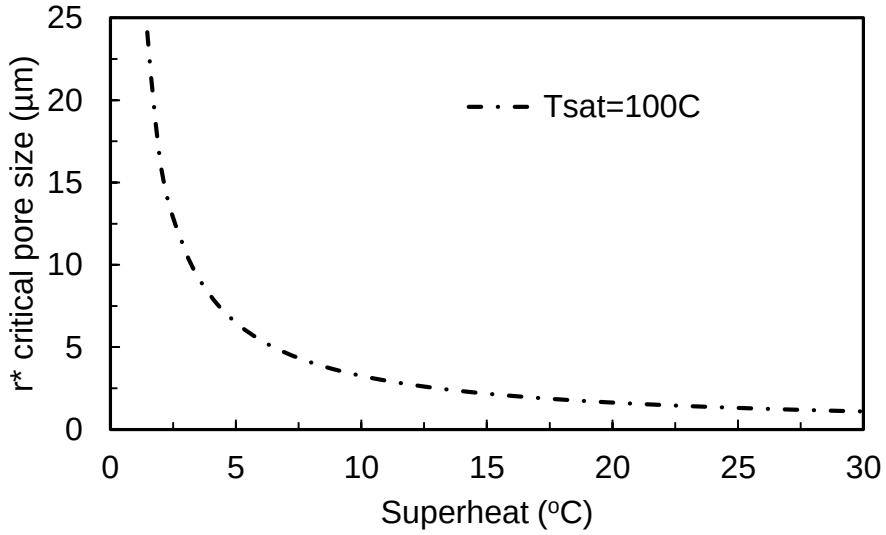

Figure 4.13 Critical pore size required for nucleation at T_{sat}=100°C

4.3.3.1 Cu-HTCMC

Figure 4.14 shows the SEM images of Cu-HTCMC made of four particle sizes: 10 μm, 25 μm, 50 μm and 85 μm, and Figure 4.15 shows the cross-sectional views of 10 μm and 50 μm size coatings. In Figure 4.14, the size of the cavities increases proportionately with increase in average particle size of each coating. At higher magnification (not shown), the smaller particles are seen to be agglomerated due to flow of brazing paste. The cross-sectional view in Figure 4.15 reveals that the cavities in the coating are of the

re-entrant type, and the smaller particles are fused together due to high temperature to make a relatively larger cavity than would be commensurate with average particle size.

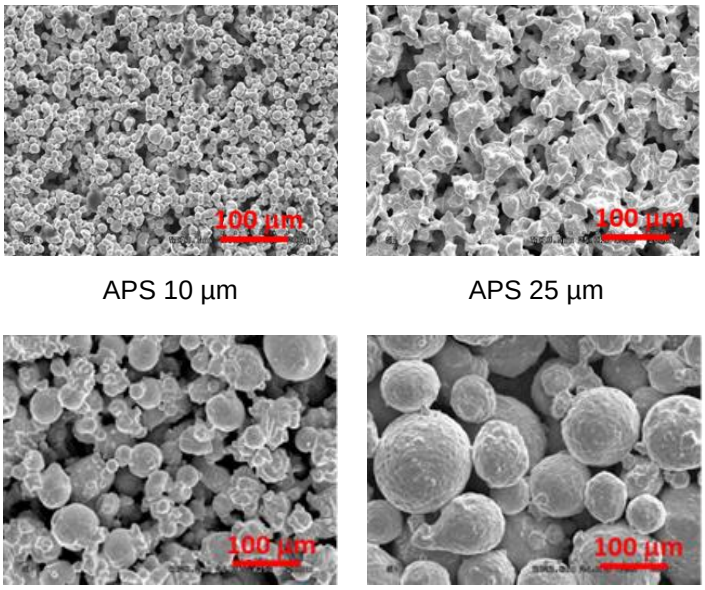

APS 10 µm APS 25 µm

APS 50 µm APS 85 µm

Figure 4.14 SEM images of Cu-HTCMC with different particle sizes

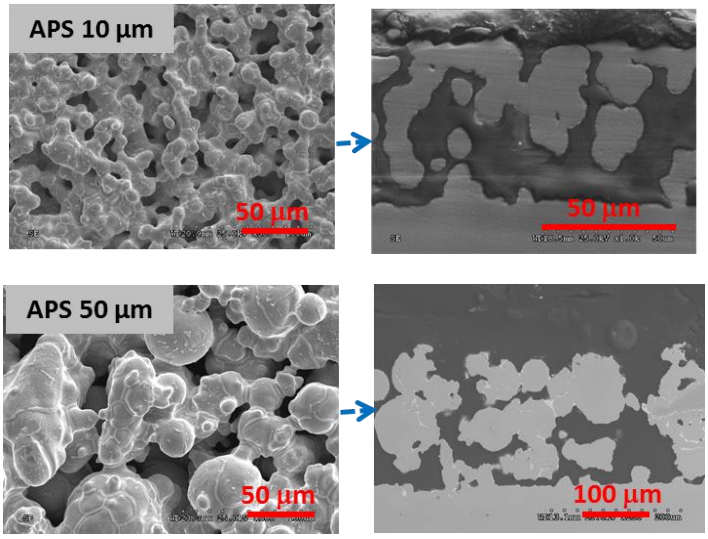

Figure 4.15 SEM images of 10 µm (top) and 50 µm (bottom) Cu-HTCMC showing their cross-sections

Figure 4.16 shows the pool boiling curves obtained with Cu-HTCMC of different particle sizes with the same thickness (160 µm). The same thickness ensures no difference in thermal resistance of the coating and allows the valid comparisons of particle size effect alone. The figure clearly shows that 50 µm size is optimal for pool boiling of water. As the particle size is decreased from 50 µm to 10 µm, the boiling heat transfer degrades sequentially. The lower enhancement given by the smaller sizes (25 µm and 10 µm) can be explained by the relationship already discussed (Equation (1-1)), between bubble embryo radius, r_b, and interfacial pressure difference, P_v-P_l, required to sustain the embryo and in turn to make it grow. Thus, higher superheats at given heat fluxes are required to activate cavities in 10 µm and 25 µm size coatings, thus lowering heat transfer coefficient. The performance of these coatings could also have been hindered by increased hydraulic and vapor removal resistance, because the ratio of coating thickness to average particle size in these coatings were significantly high: 7 to 1 for 25 µm particle size and 16 to 1 for 10 µm particle size. However, the lower performance of the largest size coating (85 µm) could be due to the ratio of coating thickness to average particle size is less than 3 to 1, meaning the thickness is insufficient to form reentrant type cavities.

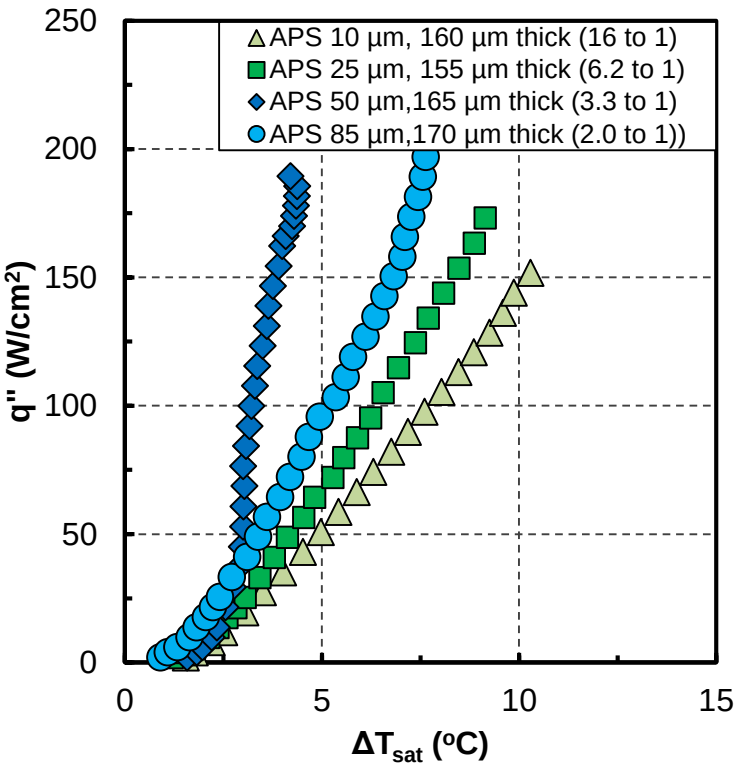

Figure 4.16 Effect of particle size on pool boiling performance of Cu-HTCMC (same thickness)

Figure 4.17 shows the pool boiling curves of Cu-HTCMC with different particle sizes with proportional thickness. Coating thickness was aimed to be 3-4 times the particle size except for 10 µm particles. The 10 µm particle coating could not be fabricated less than 75 µm thick using the current painting technique because larger brazing particles (~44 µm) present in the binder made it difficult to spread the mixture on the substrate sufficiently prior to brazing process. Nevertheless, all particle size coatings demonstrated similar heat transfer enhancement unlike what was observed in the previous results in Figure 4.16. The improvement in the heat transfer enhancement for the smaller particle size coatings (10 and 25 µm) is because of the reduced thermal resistance. Moreover, agglomeration and fusion of particles allowed these particles size coatings to possess relatively larger cavities than what would be formed from particles bonding alone (example shown in Figure 4.15).

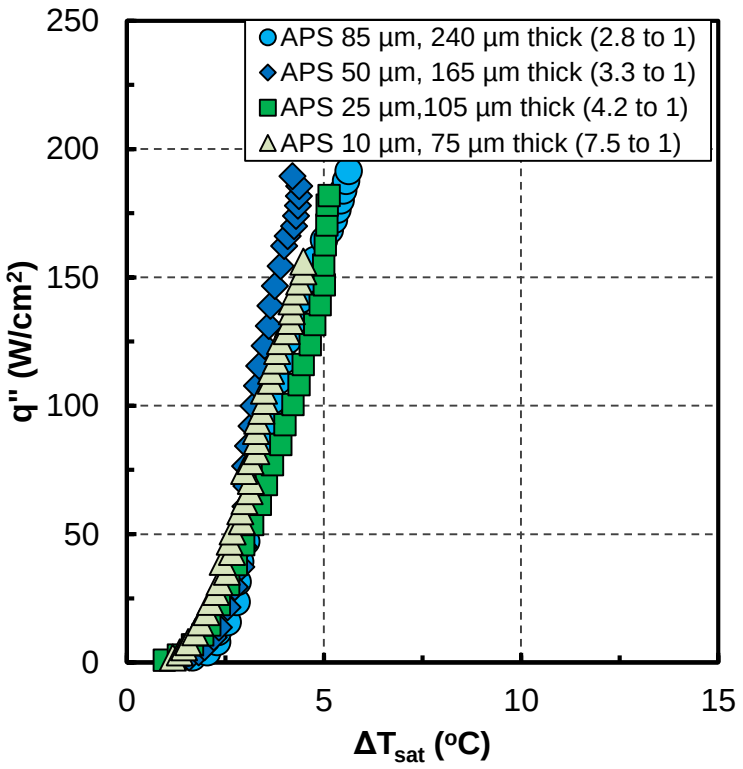

Figure 4.17 Effect of particle size on pool boiling performance of Cu-HTCMC Al-HTCMC

Figure 4.18 shows SEMs of Al-HTCMC made of four particle sizes: 10 µm, 25µm, 65 µm and 110 µm, and Figure 4.19 shows their cross-sectional views. The cavity sizes are larger for larger particle sizes. Unlike Cu-HTCMC, the smaller particles do not seem to agglomerate as much. This is partly because the brazing paste doesn't flow as well as silver brazing paste flows on copper due to inevitable oxide formation on aluminum surface. The ratio of thickness to average particle size was kept close to 3 to 1 for each coating except smaller size particles, 10 µm and 25 µm. Thickness for 10 µm particle could not be reduced to less than 100 µm because of the particles contained in the brazing paste were no less than 80 µm in diameter.

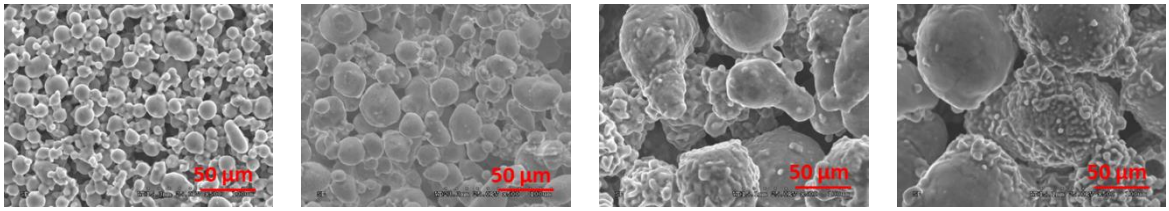

APS 10 µm APS 25 µm APS 65 µm APS 110 µm

Figure 4.18 SEM images of Al-HTCMC with different particle sizes

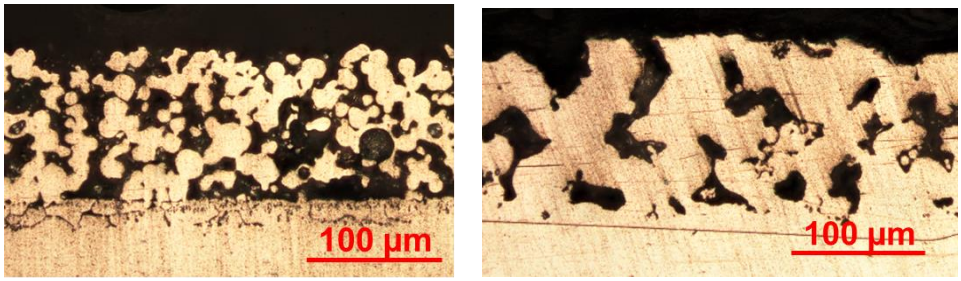

APS 10 µm APS 25 µm

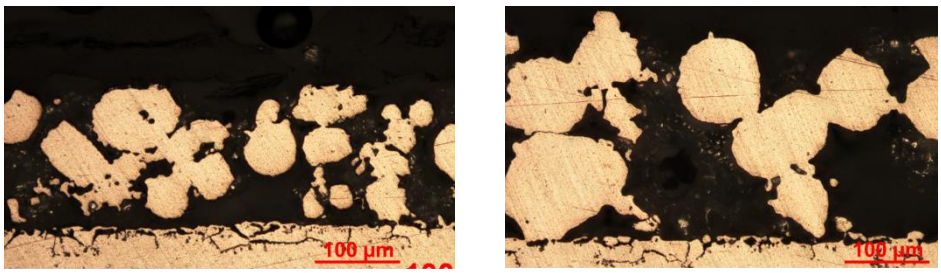

APS 65 µm APS 110 µm

Figure 4.19 Cross-sectional views of Al-HTCMC made of different particle sizes

Figure 4.20 illustrates the pool boiling results of Al-HTCMC of different particle sizes. In the figure, 25 µm particle size coating performed the best compared to all other particle sizes tested. The boiling heat transfer for 65 µm and 110 µm particle size coatings degraded significantly at higher heat flux. Thermal resistance is dominant at higher heat flux regime and for larger particle size coatings, thickness was higher as the particle size increases. However, in the case of 10 µm coating, superheats at lower heat flux region are much larger than for other size coatings, but near the CHF region, the slope of the curve changes to

steeper as the heat transfer rate improves slightly. The initial degradation of the boiling heat transfer is due to smaller cavity size and the thickness to particle size ratio being much greater, 10 to 1. Even though the thermal resistance is the least for this coating, because of the greater thickness to particle size ratio, vapor removal resistance is higher and that results into worse boiling performance.

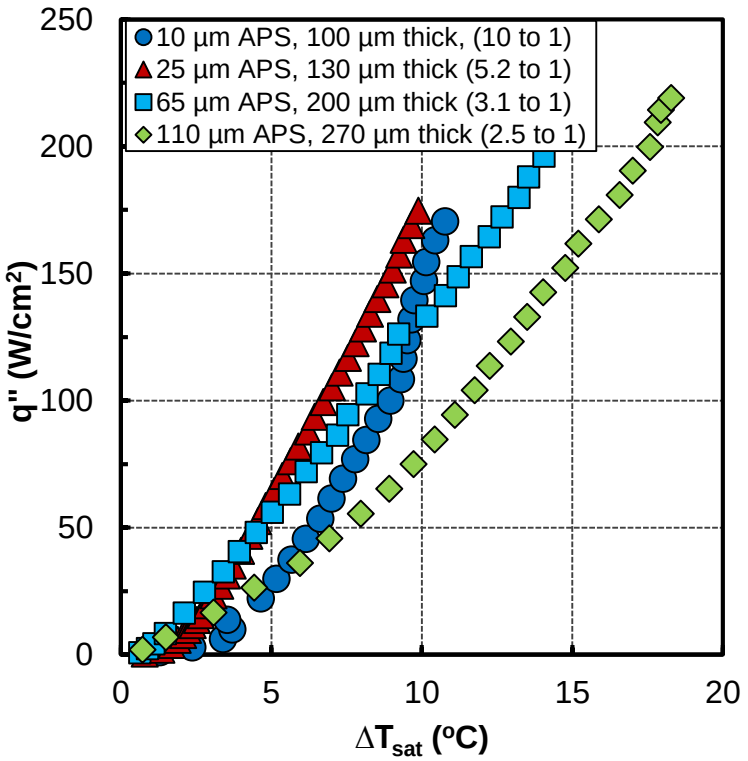

Figure 4.20 Effect of particle size on pool boiling performance of Al-HTCMC

4.4 Comparison with Other Microporous Coatings and Plain Surface

The performance of Cu-HTCMC is compared with other prior microporous coatings: ABM [34], TCMC [3] and copper wire screen [7]. All these coatings are applied on a flat copper substrate. Since Al-HTCMC is fabricated on aluminum substrate, the performance of Al-HTCMC is not included in the comparison. ABM coating was fabricated following Chang and You [34] and quality of the coating was

confirmed by repeating the pool boiling curve in FC-72, not just by comparing SEM images. TCMC coating was fabricated using copper powders instead of nickel powders following Kim [3] and the coating was able to produce better pool boiling results in water than what is reported by Kim [3]. The SEM images of ABM, TCMC, Cu-HCMC and copper wire screen are listed in Figure 4.21 for comparison. Since ABM, TCMC and Cu-HTCMC utilize the metal powders and a binder, the microstructures are similar in shape and have random distribution of cavities. In the other hand, sintered copper wire mesh shows much different microstructure with patterned pores.

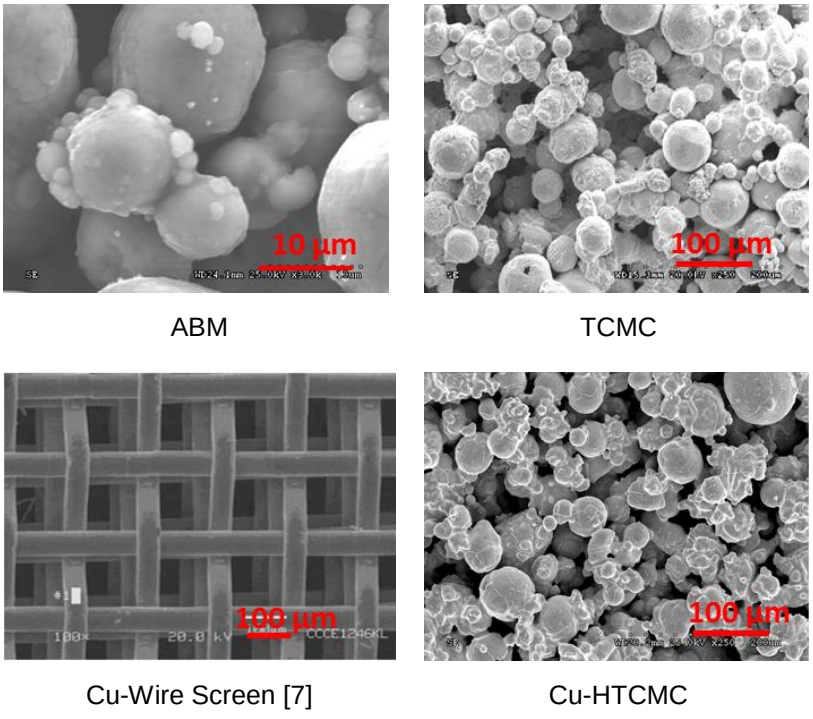

ABM TCMC

Cu-Wire Screen [7] Cu-HTCMC

Figure 4.21 SEM images of ABM, TCMC, Cu-wire screen and Cu-HTCMC

Figure 4.22 shows the pool boiling curves in water for the best performing ABM, TCMC, Cu-HTCMC and copper wire screen, and compared to the plain copper surface. Again, all the pool boiling tests were done in the same conditions and using same heater size. The data for copper wire screen is obtained from

Li and Peterson [7] and the conditions of their tests are identical to current study except that heater size is slightly smaller, 8 mm x 8 mm, compared to 10 mm x 10 mm heater size used in this study. Figure 4.22 clearly shows how effectively Cu-HTCMC enhances the pool boiling heat transfer of water compared to all other coatings. The superheats for the Cu-HTCMC coatings are much lower. In fact, the superheats for Cu-HTCMC remain below 5 ^{o}C for the full range of heat flux tested. The highest superheat it reaches at CHF of 185 W/cm^2 is ~4.3 ^{o}C, while superheat for the same heat flux for TCMC is ~7 ^{o}C and that for copper wires screen exceeds 10 ^{o}C. The superheats for ABM coating, on the other hand, is much higher and closer to the plain copper surface, which steadily increase to well beyond 10 ^{o}C after 50 W/cm^2. It should be noted that the test for ABM coated surface was not carried out up to CHF because of the temperature limitation of the epoxy that is used in the coating.

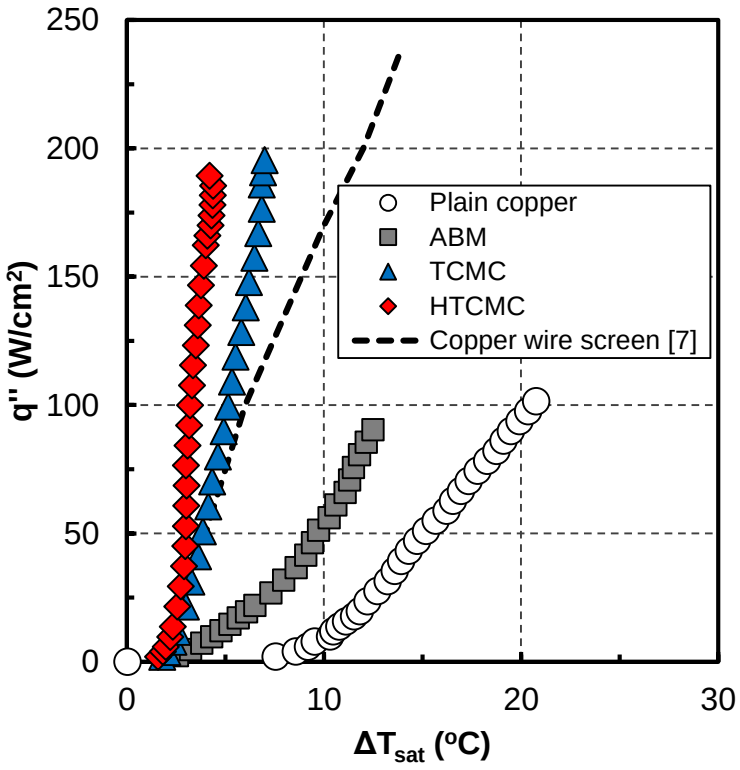

Figure 4.22 Comparison with other microporous coatings

Figure 4.23 indicates that the heat transfer coefficient from Cu-HTMC is superior to all other coatings. Near 100 W/cm^2, Cu-HTCMC increases the heat transfer coefficient ~6.3 times relative to that of the plain copper surface, while TCMC, copper wire screen and ABM increase it only 4.0, 3.4 and 1.5 times, respectively. Cu-HTCMC further increases the heat transfer coefficient as the heat flux increases, to a value of ~425,000 W/m^2-K at CHF, which is ~8.7 times that of plain copper surface at CHF. This is the unusually high heat transfer coefficient for pool boiling of water.

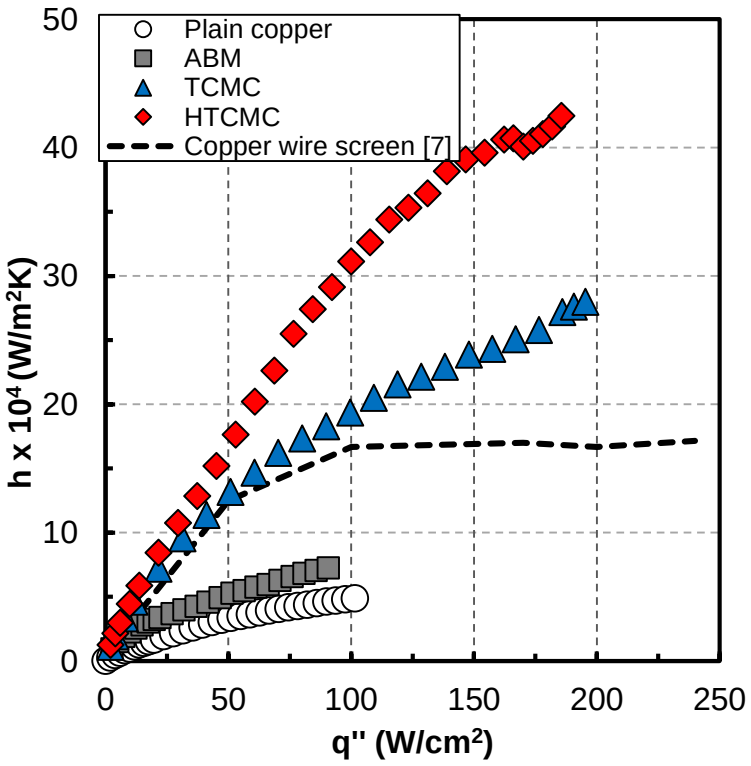

Figure 4.23 Comparison of heat transfer coefficients of other microporous coatings with Cu-HTCMC

Figure 4.24 illustrates the significant enhancement of pool boiling heat transfer achieved from the best performing Al-HTCMC, compared to plain aluminum surface. As shown in the figure, the superheats

for Al-HTCMC remain below 10 ^{o}C for the full range of heat flux tested while those for plain aluminum exceed 30 ^{o}C. Overall, there is 13-23 ^{o}C reduction in superheats in 50-175 W/cm^2 heat flux range.

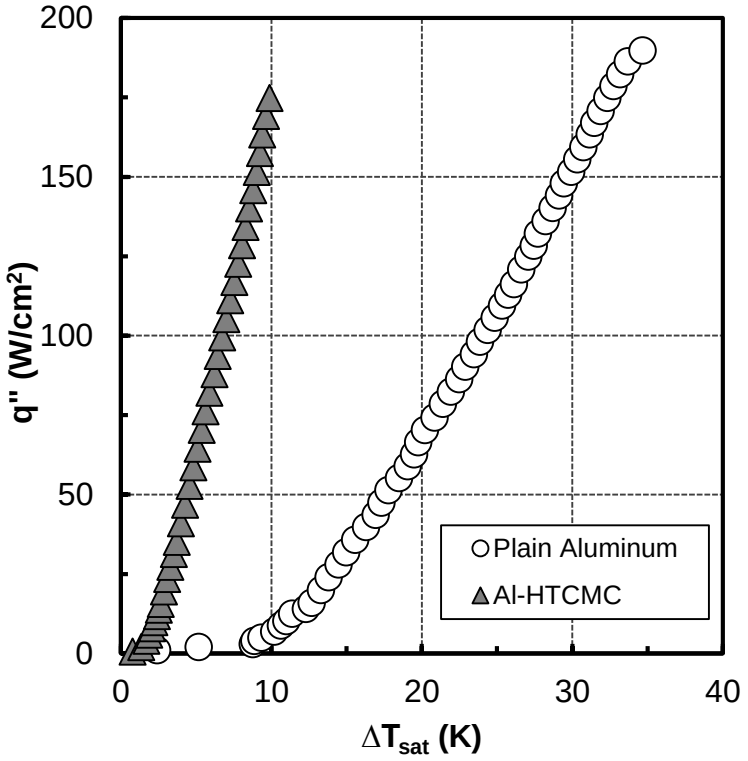

Figure 4.24 Comparison of boiling performance of Al-HTCMC with plain aluminum surface

Figure 4.25 shows the heat transfer coefficients obtained from optimal Al-HTCMC and plain aluminum surface. The figure clearly demonstrates the efficiency of Al-HTCMC in boiling heat transfer of water compared to plain surface. Near 100 W/cm^2, Al-HTCMC enhances the heat transfer coefficient ~3.5 times relative to the plain aluminum surface. Al-HTCMC further enhances the heat transfer coefficient as heat flux increases, up to ~180,000 W/m^2-K at CHF.

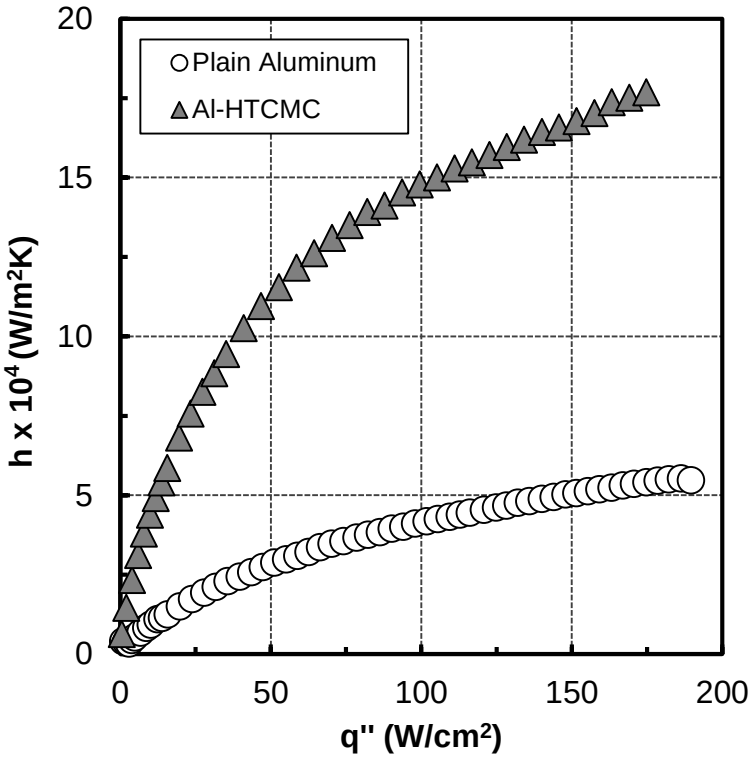

Figure 4.25 Heat transfer coefficients of Al-HTCMC and plain aluminum surface

CHAPTER 5

ENHANCEMENT OF POOL BOILING HEAT TRANSFER OF WETTING FLUILDS USING ALUMINUM MICROPOROUS COATING

Even though water has excellent thermal properties for better heat transfer, use of water as a working fluid in electronics cooling can be limited due to many reasons. The main two reasons are the high saturation temperature (100 ^{o}C) at atmospheric pressure and high freezing point (0 ^{o}C) of water. Since the operating temperature of the most of the electronic system is below 100 ^{o}C, two-phase (liquid-vapor) cooling using water as working fluid becomes impractical. Therefore, refrigerants such as HFE-7100 and acetone are often used as cooling liquid for electronics cooling system. These fluids have much lower saturation temperatures as well as much lower freezing point than water. The selected thermal properties of acetone, HFE-7100 and water are shown in the following table.

Table 5.1 Thermo-physical properties of water, acetone and HFE7100 at 1 atm

Fluid	T_{sat} (^{o}C)	ρ_l (kg/m^3)	c_p (kJ/(kg-K))	k (W/m-K)	h_{lv} (kJ/kg)	$\sigma x10^{-3}$ (N/m)
Water	100	998	4.20	0.60	2,270	72.7
Acetone	56	791	2.16	0.18	552	23.7
HFE-7100	61	1492	1.17	0.07	112	13.6

It is also well known that water is not desirable to use with any devices made of aluminum because water promotes corrosion. Instead, Acetone and HFE-7100 are often used as heat transfer fluids with aluminum devices. Therefore, it is imperative to evaluate the boiling performance of Al-HTCMC on these wetting fluids. As the surface tension of the fluid changes, it requires different pore size in the coatings to induce nucleation. Thus, the Al-HTCMC, optimized for water, is reevaluated with different particle sizes for acetone and HFE-7100.

Based on the study of ABM in FC-72 and R-123a by Kim [3], smaller range of aluminum particles, from 5 µm to 25 µm, were selected for pool boiling tests of Al-HTCMC in acetone and HFE-7100. Al-HTCMC coatings were fabricated onto the 1x1 cm aluminum test heater and tested in acetone and HFE-7100 at atmospheric pressure. Their pool boiling results are presented in this chapter.

5.1 Acetone

5.1.1 Plain Aluminum Reference curve

Two separate plain aluminum heaters were tested in pool boiling of acetone to obtain a reference curve. The plain aluminum surface was polished on 600 grit paper and the roughness was measured to be 0.3 µm. Two pool boiling curves for plain aluminum are shown in Figure 5.1. In the figure, both pool boiling curves are nearly identical, showing the repeatability of the data measurement. These results for plain aluminum surface are also compared with an experimental data obtained from Rao et al [35] for the same surface. As shown in the figure, the boiling heat transfer results of the current data match with that from Rao et al. except the heat flux limit. Current results show that CHF is about ~41 W/cm^2, which is just 13% higher than that predicted by Zuber's correlation [14]. It should be noted that Rao et al. [35] did not specify whether the test results include CHF or not. Moreover, the heater size used in their study was almost 7 times larger than the current test surface area. CHF decreases with the heater size [30] [36] which might be the reason for shorter pool boiling curve from Rao et al. [35]

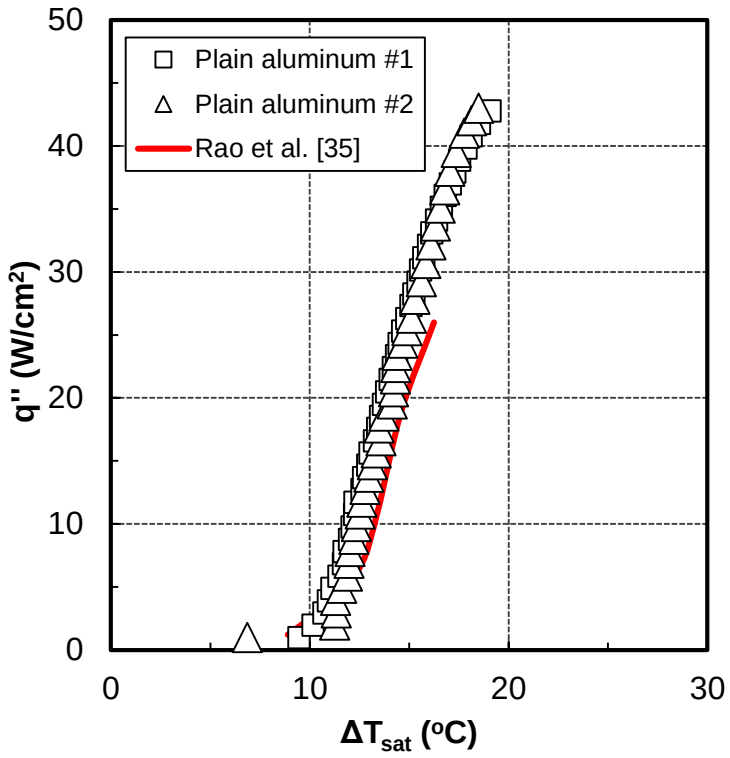

Figure 5.1 Reference pool boiling curve for plain aluminum in acetone

5.1.2 Al-HTCMC

Figure 5.2 illustrates the pool boiling curves of Al-HTCMC coated surfaces immersed in saturated acetone at atmospheric pressure. In addition, a nucleate boiling curve of plain aluminum surface is also shown for reference. The single-phase natural convection data of all the surfaces including plain surface exhibit constant and equal heat transfer coefficients indicating equivalent areas and showing negligible surface microstructure effects. The incipient superheat value of the largest particle size, 25 μm, is the lowest and this value increases as the particle size decreases. This phenomenon can be explained by equation (5-1).

$$\Delta T_{sat} = T_w - T_{sat\ @\ P_l} = \frac{2\sigma}{r_b}\left(\frac{T_{sat\ @\ P_l} \times v_{lv}}{h_{lv}}\right) \quad (5\text{-}1)$$

For a given working fluid at certain pressure, the liquid properties are fixed and the required superheat to initiate liquid vaporization at the liquid-vapor interface is dependent only on, and inversely proportional to, the embryonic bubble radius, r_b. Therefore, the more vapor trapped in a cavity, the larger the embryonic bubble radius and the lower superheat required to initiate bubble growth.

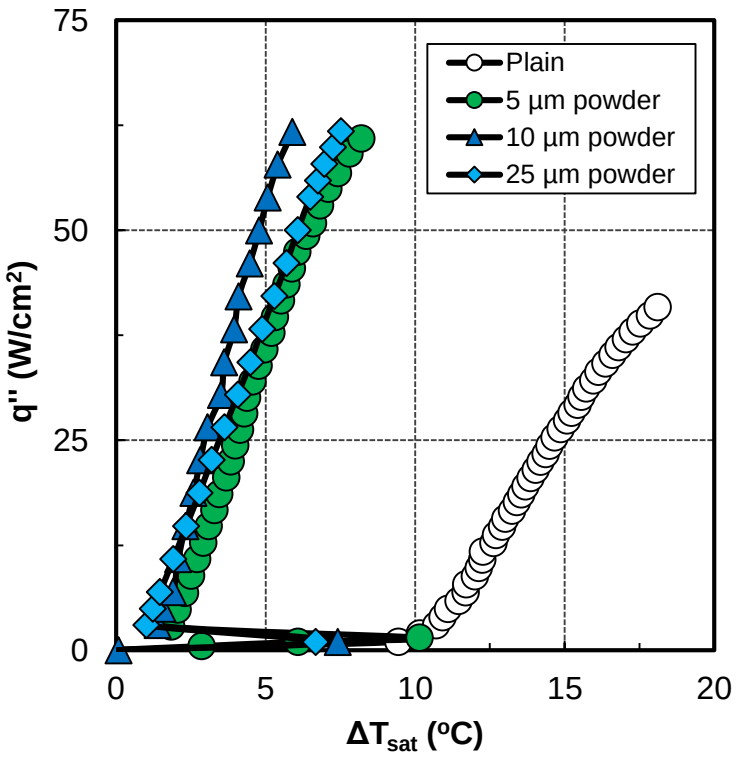

Figure 5.2 Pool boiling results of Al-HTCMC in saturated acetone

The surface microstructure effect on nucleate boiling heat transfer and CHF can be clearly seen in Figure 5.3. In general, all particle sizes of Al-HTCMC show a huge enhancement of nucleate boiling heat transfer and CHF over a plain surface at entire heat flux range. The 10 µm size coating shows the best

enhancement for the nucleate boiling, ~370%, while 25 µm and 5 µm size coatings show 270% and 260% enhancement for the nucleate boiling, respectively. The enhancement of CHF by all particle sizes is ~50% relative to plain aluminum surface.

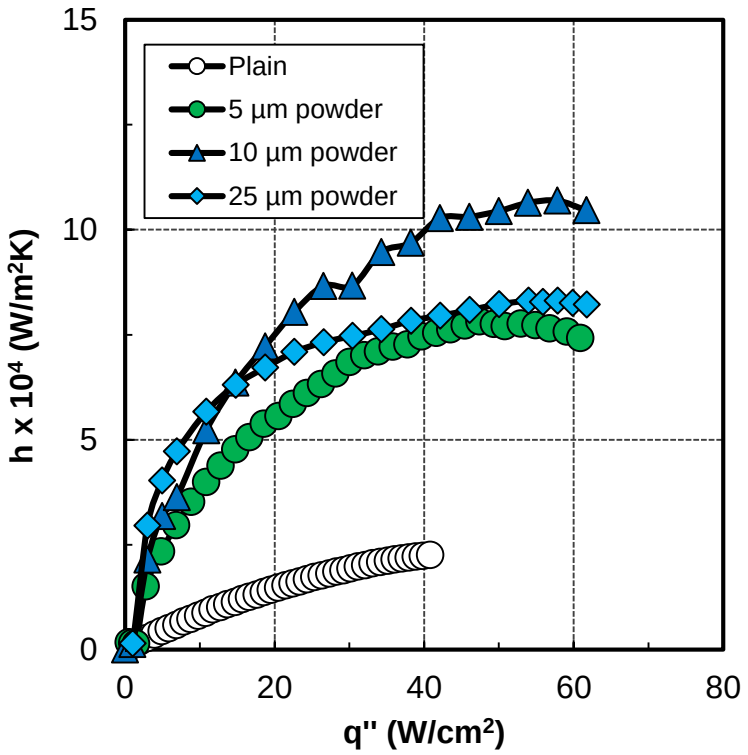

Figure 5.3 Boiling heat transfer coefficient of Al-HTCMC in saturated acetone

5.2 HFE-7100

5.2.1 Plain Aluminum Reference Curve

Figure 5.4 shows the pool boiling curve for plain aluminum surface (sanded on 600 grit paper) for reference. The curve is compared to the pool boiling results of plain copper surface (sanded on 2000 grit paper) from Thiarajan [28]. The discrepancy between the heat transfer results between plain aluminum and

plain copper might be due to the difference in surface roughness, rather than substrate conduction only. CHF for the plain aluminum surface falls within 10% of Zuber's prediction.

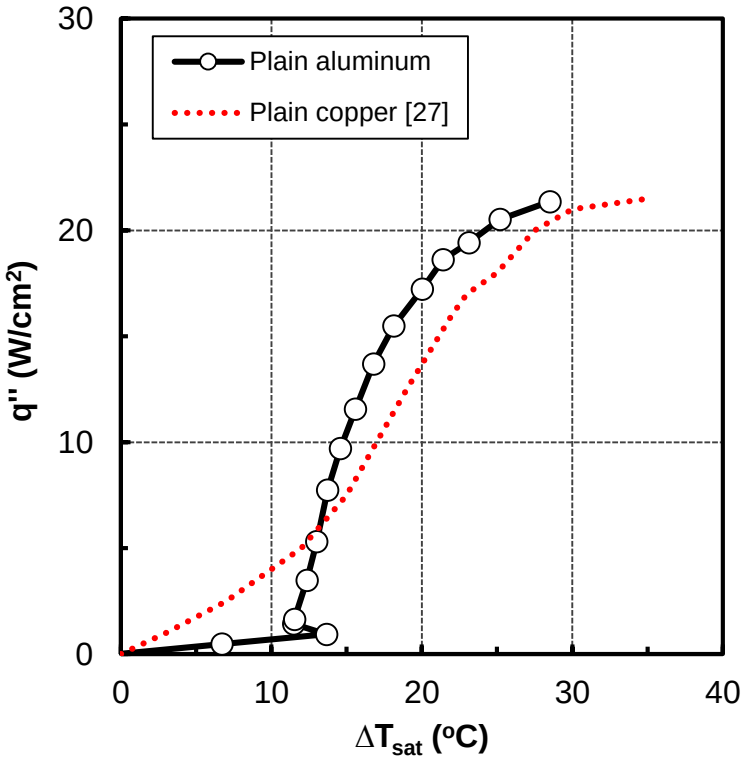

Figure 5.4 Pool boiling curve for plain aluminum in saturated HFE-7100

5.2.2 Al-HTCMC

Figure 5.5 shows the pool boiling curves of the plain aluminum and Al-HTCMC coated surfaces immersed in saturated HFE-7100 at atmospheric pressure. Again, the natural convection data of all of the surfaces exhibit identical heat transfer coefficients indicating equivalent areas and showing negligible surface microstructure effects. Also, the incipience superheat for the largest particle size is the lowest and it increases with decrease in particle size, which is consistent with what was observed in the case of

acetone. In overall, Al-HTCMC coatings showed less than 10 ^{o}C wall superheats, while plain aluminum surface, the superheats was closer to 30 ^{o}C near CHF (21 W/cm^2).

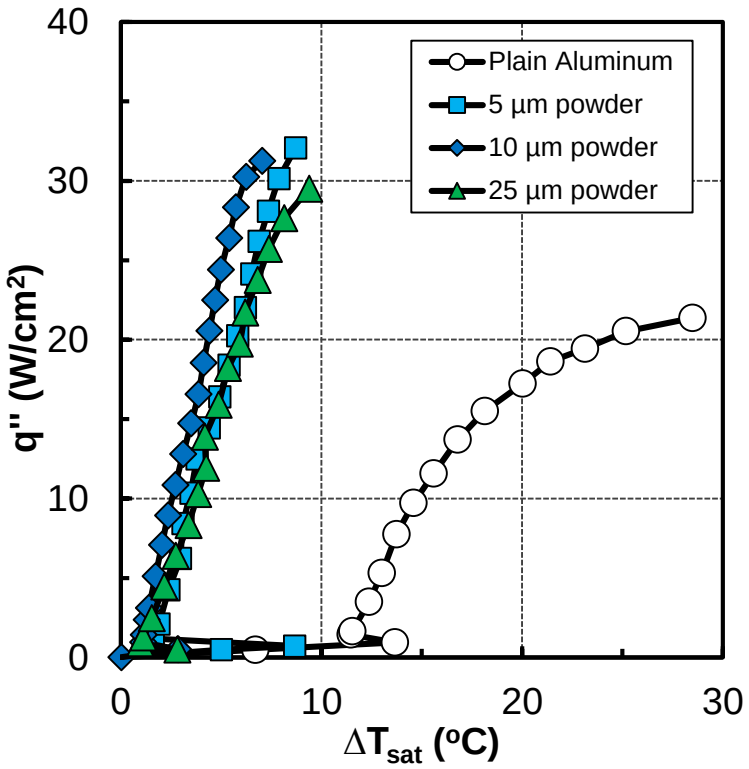

Figure 5.5 Pool boiling curves of Al-HTCMC in saturated HFE-7100

Boiling heat transfer coefficients of plain aluminum and Al-HTCMC coated surfaces immersed in saturated HFE-7100 are shown in Figure 5.6. In the figure, all particle size Al-HTCMC coatings show significant enhancement in nucleate boiling heat transfer and CHF compared to plain surface. Among three sizes coatings tested, again, 10 µm size coating shows the maximum enhancement, ~460% for the nucleate boiling, while 5 and 25 µm size coatings show only 330% and 300% enhancement for nucleate boiling heat transfer, respectively. The enhancement of CHF is ~50% relative to plain aluminum surface for all particle sizes.

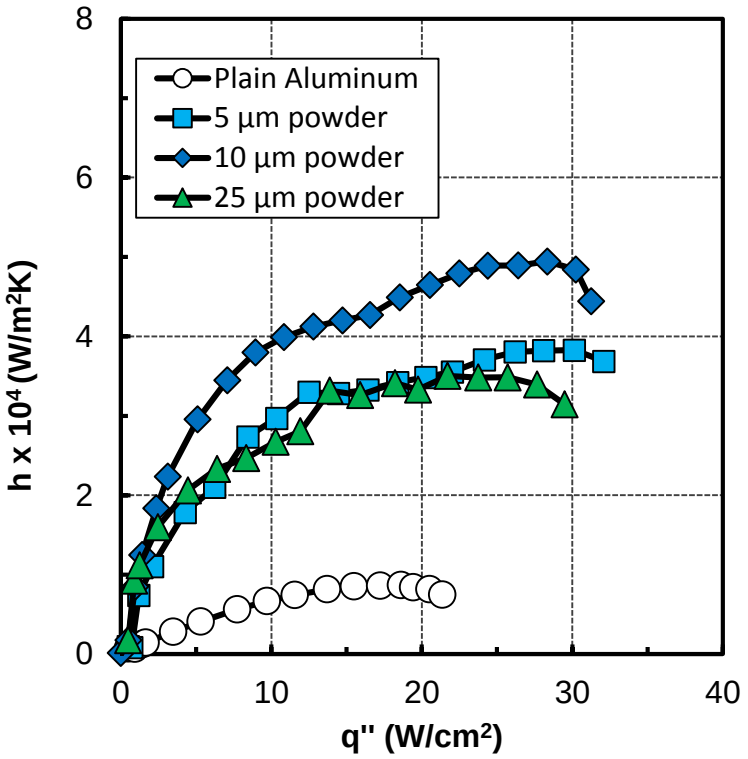

Figure 5.6 Boiling heat transfer coefficients of Al-HTCMC in saturated HFE-7100

CHAPTER 6

ENHANCEMENT OF EVAPORATIVE HEAT TRANSFER USING ALUMINUM MICROPOROUS COATING

Spray cooling and jet-impingement cooling are highly efficient means of high heat flux dissipation and hence used in many applications such as metal casting fabrication, laser cooling, and power electronics cooling. The high efficiency of the heat transfer for these two techniques comes from the phase change, primarily evaporation, combined with the single phase forced convection. The finely atomized droplets of the sprays in addition to the thin liquid films promote evaporation. In addition to evaporation, higher heat fluxes can produce nucleation which further increases heat dissipation.

Although it has been known that in spray and jet-impingement cooling processes, heat can be dissipated in the ways of film evaporation, forced convection, and nucleate boiling [37] [38] [39], the dominant mechanism depends on the wall superheats. At low wall superheats, the heat dissipation is mainly contributed by the forced convection and the evaporation from the free surface of the thin liquid film [38] [39]. In this case, the thin liquid film is the main heat transfer resistance so that a thinner liquid film is very desirable. However, in the case of higher wall superheats, the thin liquid film is broken to form liquid blocks [40] and if film is thick, nucleate boiling becomes the main mechanism of heat transfer.

To improve the spray and jet-impingement cooling performance at all heat flux levels, surface properties become critical. Ideal surface should be able to spread the liquid into thin film, have higher heat transfer area and should produce sufficient nucleation sites. Considering these facts, a variety of surface enhancement techniques have been successfully developed. Hsieh and Yao [39] fabricated micro-sized square fins onto silicon surfaces and reported heat transfer enhancement for spray cooling using water. They associated this enhancement to the capillary force of the structured surface spreading the liquid into thin film. Micro-pin fins are also used for heat transfer enhancement of jet-impingement cooling [41]. Similarly, Yang et al. [42] fabricated microcavity surfaces to enhance the spray cooling performance with

ammonia. They demonstrated significantly high heat transfer coefficient up to ~148,000 W/m^2K at 451 W/cm^2. Besides the use of these highly structured surfaces, microporous coatings are also used for spray and jet-impingement cooling enhancement. Kim et al. [43] used low-thermally conductive microporus coatings (ABM) to evaluate their spray cooling performance at relatively low flow rates (≤ 3 ml/min of water) and showed enhancement in heat transfer coefficients up to 400% compared to dry air cooling with plain surface. This enhancement was attributed to the wicking effect of the coating. However, the experiment was conducted up to very low heat flux (≤ 5 W/cm^2). Moreno [6] later utilized more conductive microporous coating (TCMC) for the spray cooling enhancement using FC-72. He was able to compare the spray cooling performance of FC-72 between TCMC and ABM coatings and showed that TCMC performed better than ABM coating for the same test conditions. Higher thermal conductivity of TCMC was believed to be the factor for the better enhancement relative to ABM. Since forming thin liquid film is critical for evaporation, surface wettability is also important, especially when the working fluid is non-wetting, such as water. Although surface wettability of ABM and TCMC for water were not reported by Kim [43] and Moreno [6], respectively, Malla [32] demonstrated that these coatings were actually non-wetting to water.

Al-HTCMC, described in previous sections, exhibits surface properties suitable for spray and jet-impingement cooling enhancement using water. The porous structure of the coating significantly improves the heat transfer area, and the capillary effect facilities liquid (water) to spread well on the surface. In addition to the capillary effect, Al-HTCMC, when treated with hot water, produces extremely low contact angle of water due to oxides formation (as shown in Figure 6.1), resulting in thin water film, and thus, low heat transfer resistance. These characteristics of Al-HTCMC can be extremely beneficial for thin-film evaporation. Besides, the microcavities that exist in the coating have been proven to be effective in nucleate boiling heat transfer (CHAPTER 4). This combined effect of spreading the liquid and enhanced nucleation makes Al-HTCMC a perfect candidate as a surface for spray and jet-impingement cooling enhancement. Therefore, in this study aluminum microporous coating is investigated as a means to enhance the evaporative heat transfer in spray and jet-impingement cooling. However, this study is not intended for

discovering the best spray or jet-impinging characteristics. The flow characteristics of spray cooling test were derived from Kim et al. [43] while those of jet impingement cooling were obtained from Malla [32]. For both spray and jet-impingement cooling experiments, tests were conducted using 10x10 mm aluminum heaters with Al-HTCMC coated and uncoated surfaces in ambient environment. Prior to the actual tests, both coated and uncoated surfaces were treated with hot water (~100 ^{o}C) for an hour in order to increase the wettability of water. The heater surface orientation was kept vertical to drain the excess liquid (water) by gravity, to avoid pooling the liquid on the surface.

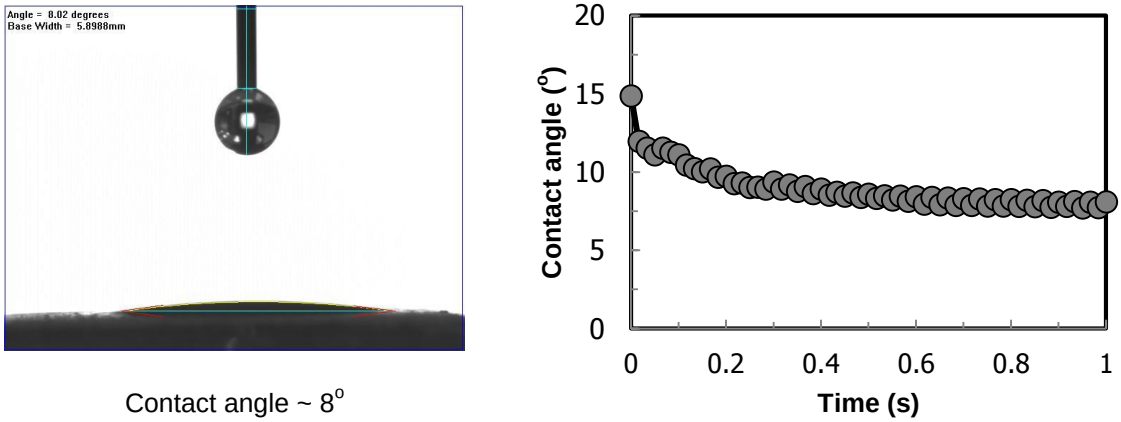

Figure 6.1: Wettability of water on Al-HTCMC

6.1 Spray Cooling

The detailed experimental setup and procedures for spray cooling experiments are given in chapter 2.5. Experiment was conducted in various flow rates which were controlled by pressure regulator. The flow characteristic of the spray is shown in Figure 6.2 with the volumetric flow rate as a function of pressure drop.

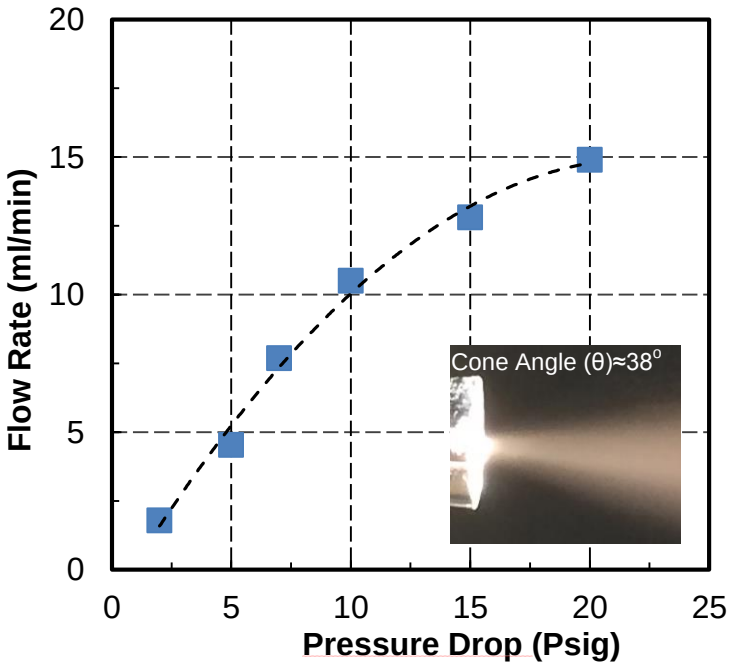

Figure 6.2 Flow characteristic of the spray

The droplet sizes produced by the spray were estimated using a correlation, equation (6-1), developed by Estes and Mudawar [44]. This correlation predicts the Sauter Mean Diameter (SMD) for full cone spray nozzles considering both the hydrodynamic and aerodynamic forces involved in the liquid atomization process.

$$d_{32}(SMD) = 3.67 * d_o\left[We_{d_o}^{0.5}\, Re_{d_o}\right]^{-0.259} \tag{6-1}$$

The Weber number and Reynolds number used in the correlation are based on the conditions at the orifice, which are defined, respectively, as

$$We_{d_o} = \frac{\rho_a (2\,\Delta P/\rho_f) d_o}{\sigma} \tag{6-2}$$

and

$$Re_{d_o} = \frac{\rho_f (2\,\Delta P/\rho_f)^{0.5}\, d_o}{\mu_f} \tag{6-3}$$

The calculated SMD values at different flow rates of the spray are summarized in Table 6.1. The droplet size in the present study is solely dependent on the pressure drop. As the pressure drop is higher, the droplet size is smaller.

Table 6.1 Calculated SMD using equation (6-1)

Flow Rate (ml/min)	**∆ P (psi)**	**d_o (mm)**	**SMD (μm)**
2.8	3	0.3	77
4.5	5	0.3	68
10.5	10	0.3	56
12.8	15	0.3	51
14.9	20	0.3	47

Prior to testing the Al-HTCMC coated heater, spray cooling tests were conducted for plain aluminum surface with different flow rates, ranging from 2.8 ml/min to 14.9 ml/min. The spray cooling curves are plotted as heat flux vs. surface temperature. From Figure 6.3, it is clear that the heat transfer rate increases with increasing flow rates. It is due to not just the higher liquid volume reaching the heated surface, but also due to the fact that smaller droplets with higher impact velocity result into the thinner liquid film on the surface, which promotes better evaporation rate. The difference in the heat transfer performance among different flow rates is more prominent at higher superheats near or above the saturation temperature (100 ^{o}C) due to significant thin film evaporation and nucleate boiling effects, while at lower superheats,

where forced convection is dominant, the heat transfer performance is increased slightly for higher flow rates. It should be noted that all the spray cooling tests were stopped prior to CHF due to the power limitation of the heater, which is 250 W.

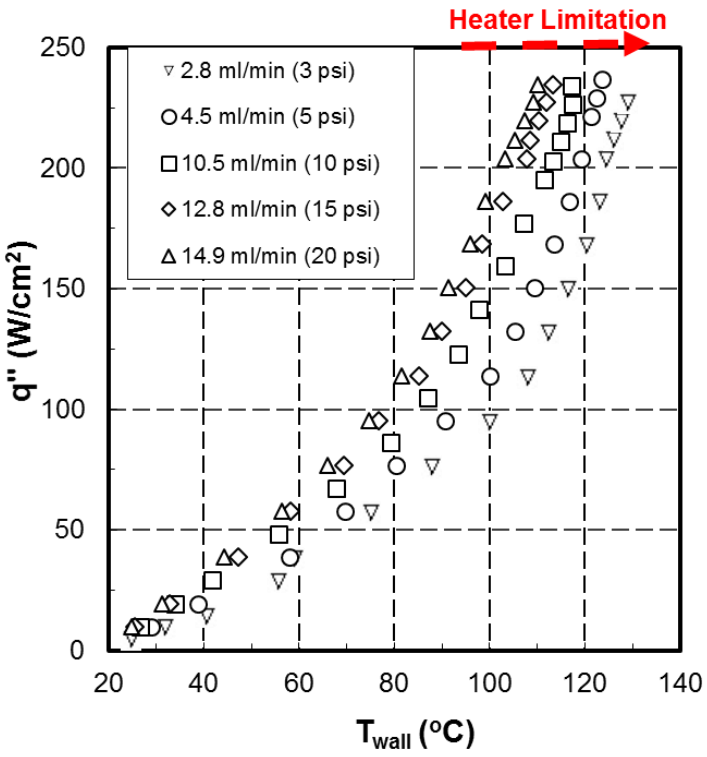

Figure 6.3 Spray cooling results of plain aluminum for different flow rates

Figure 6.4 shows the spray cooling performance for Al-HTCMC coated surface for different flow rates. Similar to plain aluminum surface, the surface temperature decreases as the flow rate increases at lower superheats due to increasing forced convection with the flow rates. However, as the superheat approaches saturation temperature, the flow rates do not seem to affect the surface temperature. This is due to the ability of microporous coating to effectively spread the liquid for all cases including when the droplet size is larger at the lower flow rate.

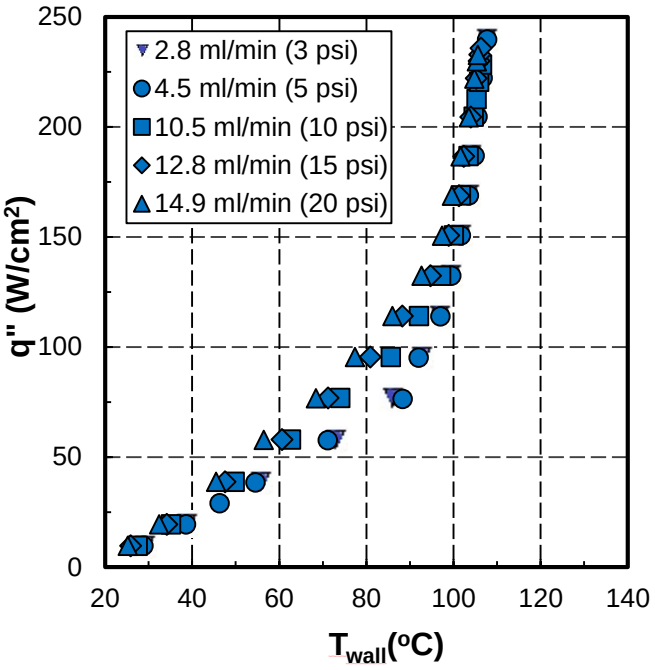

Figure 6.4 Spray cooling results of Al-HTCMC with different flow rates

The comparison of spray cooling performances between plain and Al-HTCMC coated surfaces is shown in Figure 6.5. Only the results for the lowest flow rate (2.8 ml/min) and the highest flow rate (14.9 ml/min) tested, are shown in the figure for clarity. As expected, the benefits of microporous coating is not evident in the single phase forced convection regime, regardless of flow rates. But at the regime where evaporation and nucleation is dominant, microporous coated surface shows significantly lower temperature compared to plain surface. However, as the flow rate increases, the enhancement due to microporous coating compared to plain surface gradually decreases to a point where there is no enhancement, which is seen at the highest flow rate. This is again because for higher flow rate, the droplet is sufficiently small enough such that the liquid film doesn't require much spreading to minimize its thickness.

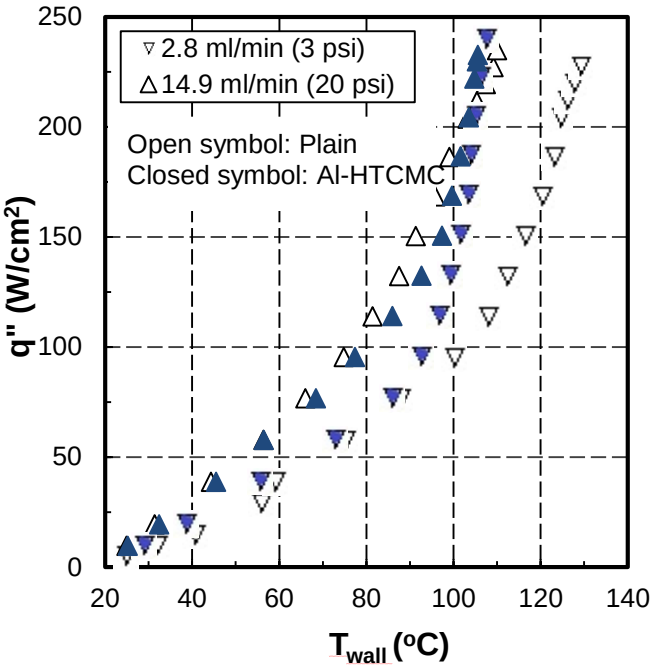

Figure 6.5 Comparison of spray cooling performance between plain aluminum and Al-HTCMC

6.2 Jet-impingement Cooling

The detailed experimental setup and procedures for jet-impingement cooling experiments are given in chapter 2.5. For these experiments, liquid is delivered on to the center of the heated surface as a pulsed jet of discrete droplets by using a solenoid valve rather than continuous jet. Based on droplet characterization by Malla [32], the droplet volume/size increases with pulse width (duration) and pressure drop. For the present study, pulse width of 0.8 ms and pressure drop of 10 psi were fixed, which dispensed 56 nl droplet. The flow rates were varied by controlling the frequency from 300 Hz to 600 Hz, and were calculated by multiplying the droplet volume by the frequency, as shown in equation (2-2). The flow rates were validated by measuring the volume of water dispensed and dividing it by the time of dispensing. The calculated flow rates for different frequencies are listed in Table 6.2.

Table 6.2 Calculated flow rates for jet-impingement cooling

∆ P (psi)	Droplet vol. (nl)	Frequency (Hz)	Flow Rate (ml/min)
10	56	300	1.0
10	56	500	1.6
10	56	600	2.0

Figure 6.6 shows the jet-impingement cooling curves, as heat flux vs. surface temperature, of plain and Al-HTCMC coated surfaces for different flow rates. Open symbol represents the cooling curves for plain surface whereas closed symbol represents that for Al-HTCMC coated surface. Unlike spray cooling tests, jet-impingement cooling tests were conducted up to CHF, which is represented by an arrow in the cooling curve. Similar to the results of spray cooling, the effect of flow rate on the surface temperature is distinct for plain surface at both single phase convection and phase change regimes, while the same effect is negligible for Al-HTCMC coated surface at the two-phase regime. This is because of the ability of microporous coatings to spread the liquid to wet the entire surface for all flow rates while excess liquid is drained by gravity. For plain surface, the surface temperature is lower for higher flow rates, especially in the two-phase regime which means the heat transfer coefficients increases with flow rates. This is because when the liquid is impinged at the center of the surface, only part of plain surface near the center is wetted with liquid due to splashing and this wetted area increases with higher flow rate. From the figure, it is also evident that CHF is also increased with increasing flow rates for both plain and Al-HTCMC coated surfaces because of the higher frequency of liquid delivery to the surface to replenish the dry zones.

For the same flow rate, Al-HTCMC coated surface showed significant enhancement in both heat transfer coefficient and CHF compared to plain surface. At the CHF of plain surface for each flow rate, the surface temperature was less by 20 ^{o}C or more on Al-HTCMC coated surface. In addition, CHF was enhanced significantly by Al-HTCMC. The maximum enhancement in CHF was up to 54% at the lowest flow rate, 1.0 ml/min, while the minimum enhancement in CHF was ~25% for highest flow rate, 2.0 ml/min.

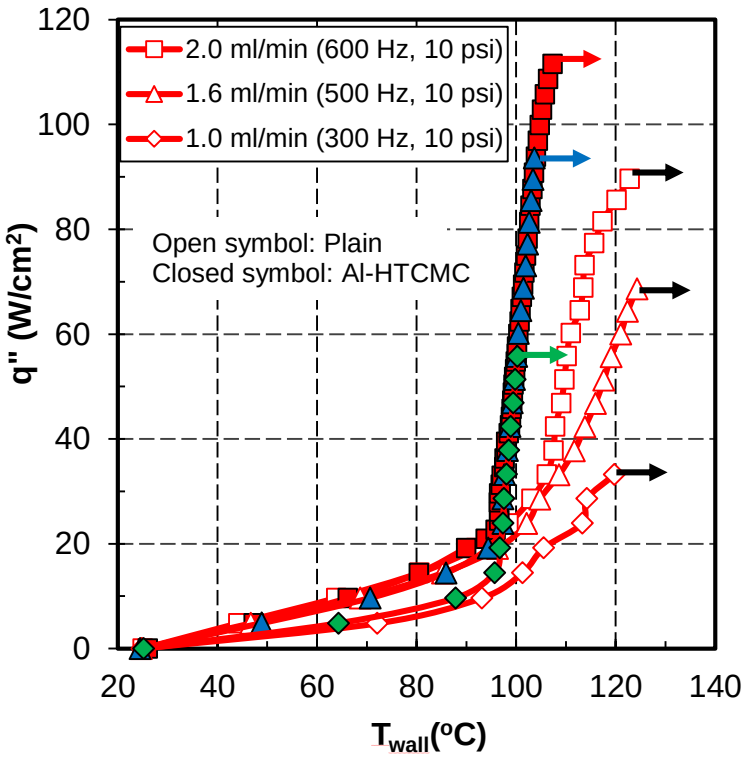

Figure 6.6 Jet impingement cooling results for plain and Al-HTCMC for different flow rates

CHAPTER 7

CONCLUSIONS AND RECOMMENDATIONS

7.1 Conclusions of CHAPTER 4: Pool Boiling Performance of Cu-HTCMC and Al-HTCMC in Water

1. The development of high temperature thermally conductive microporous coatings, Cu-HTCMC and Al-HTCMC, are conducted to upgrade the performance and reliability of ABM and TCMC, while maintaining a similar fabrication technique. Each coating is optimized for its composition, thickness and particle size to achieve the best possible combination of these parameters for pool boiling heat transfer of water.

2. The optimized Cu-HTCMC shows significantly lower wall superheats compared to plain copper surface. In fact, the highest wall superheat it reaches for 0 to 185 W/cm^2 heat flux range is only 4.3 ^{o}C, i.e. the variation of wall superheat with the heat flux input is only 0.02 ^{o}C/(W/cm^2). The optimized Al-HTCMC also shows substantial reduction in wall superheat compared to plain aluminum surface. When the heat flux range is from 0-170 W/cm^2, the highest wall superheat remains below 10 ^{o}C, while wall superheat easily exceeds 30 ^{o}C for plain aluminum surface. The performance difference between Cu-HTCMC and Al-HTCMC is believed to be mostly due to the difference in thermal conductivity of the materials.

3. Cu-HTCMC shows significant enhancement in boiling heat transfer coefficient, by about 500% at the heat flux equal to the CHF of plain surface. The heat transfer coefficient of Cu-HTCMC further increases with heat flux, up to ~425,000 W/m^{2}K, which is ~8.7 times that of plain copper surface at CHF. Cu-HTCMC also outperformed other microporous coatings such as ABM, TCMC and sintered copper wire screen. On the other hand, the maximum enhancement in boiling heat transfer coefficient by Al-HTCMC is about 280%, which occurs at around 50 W/cm^2. The highest heat transfer coefficient achieved by Al-HTCMC is ~180,000 W/m^{2}K, which is ~ 3.5 times the highest value achieved by plain aluminum surface.

4. CHF is nearly doubled by Cu-HTCMC compared to plain copper surface. However, that is not the case for Al-HTCMC. Since plain aluminum surface itself enhances CHF, due to its high surface wettability, CHF is not further enhanced by Al-HTCMC. The increased surface wettability of the plain aluminum is believed to be associated with formation of oxides and hydroxides on the aluminum surface during boiling in water.

5. Experimental results indicate that mixing ratio of 2.8:1 (powder to binder) leads to the best boiling heat transfer performance for Cu-HTCMC, while the optimum ratio for Al-HTCMC is found to be 1:1. SEM images of the coatings and cross sections reveal that when the ratio is decreased, pores are clogged with binder material. When the ratio is increased, the porosity is increased to the point where liquid can flood the cavities diminishing trapped vapor. Both effects lead to reduced nucleation sites, and consequently to worse boiling heat transfer performance.

6. For Cu-HTCMC, the coating thickness to average particle size ratio is found to be a critical factor, rather than thickness or particle size alone. For the range of particle sizes tested, coating thickness of 3-4 times the average particle size produced maximum boiling heat transfer irrespective of particle size. Due to agglomeration and fusion when particles are smaller, smaller particle coatings have cavities larger than would be commensurate with average particle size. Because of this, along with the reduced thickness, the smallest or 10 μm particle size coating showed same magnitude of enhancement as larger particle size coatings. However, for Al-HTCMC, 25 μm particle size coating showed the best boiling performance compared to all other particle sizes investigated.

7.2 Conclusions of CHAPTER 5: Enhancement of Pool Boiling Heat Transfer of Acetone and HFE-7100 using Al-HTCMC

1. In general, Al-HTCMC, regardless of its particle size, shows notable reduction in wall superheats for both acetone and HFE-7100. The highest superheat remains below 10 ^{o}C for entire heat flux range for both fluids.

2. For acetone, the maximum enhancement in boiling heat transfer coefficient by Al-HTCMC is ~370%, while that in CHF is ~50% relative to plain aluminum surface. Similarly, for HFE-7100, the maximum enhancement by Al-HTCMC in boiling heat transfer and CHF are ~460% and ~50%, respectively.

3. For both acetone and HFE-7100, 10 μm size coating shows the best heat transfer coefficient, while all particle size coatings show similar CHF enhancement. The pool boiling results of both fluids indicate that the boiling incipience increases as the particle size decreases, but, the incipience for all particle sizes is lower than that for plain surface.

7.3 Conclusions of CHAPTER 6: Enhancement of Evaporative Heat Transfer in Spray and Jet-impingement Cooling using Al-HTCMC

7.3.1 Spray Cooling

1. The spray cooling performance on plain aluminum surface is found to be dependent on flow rates for both single phase and two-phase regimes. Increased single-phase convection and finer droplets with the increasing flow rates cause the spray cooling performance to improve as flow rate increases for plain aluminum. However, for Al-HTCMC coated surface, as heat flux range progresses to two-phase regime, the spray cooling curves of various flow rates begin to converge showing less sensitivity to flow

rate. This is because of the ability of microporous coatings to spread the liquid to wet the entire surface for all flow rates.

2. Al-HTCMC coated surface does not show any improvement in spray cooling performance in single phase regime compared to plain aluminum surface. The enhancement from Al-HTCMC is notable only in two-phase regime, where thin film evaporation and nucleate boiling is dominant.

3. The maximum enhancement in spray cooling performance due to Al-HTCMC occurs at the lowest flow rate, where droplet size is believed to be the largest. In that case, Al-HTCMC facilitates the spreading of large droplet into thin liquid film more effectively than plain aluminum surface. As flow rate increases, the spray cooling performance of plain surface nears that of Al-HTCMC coated surface because droplet size becomes small enough that the liquid spreading becomes less important.

7.3.2 Jet-impingement Cooling

4. Like in spray cooling, plain and Al-HTCMC show identical cooling curves in the single phase regime showing no enhancement from the microporous coating. However, at two-phase regime, Al-HTCMC shows significant enhancement in both evaporative heat transfer as well as CHF compared to plain surface. At the CHF of plain surface for each flow rate, the surface temperature is reduced by 20 ^{o}C or more. CHF is increased up to 54% at the lowest flow rate, however, the extent of CHF enhancement decreases with the increasing flow rate.

5. For plain surface, as the flow rate increases, the cooling performance also increases, especially in the two phase regime. This is because when the liquid is impinged at the center of the surface, only part of plain surface near the center is wetted with liquid due to splashing and this wetted area increases with

higher flow rate. However, for Al-HTCMC coated surface, there is no difference in cooling performance with the various flow rates, where the phase change is dominant. Due to higher surface wettability and capillary wicking of microporous coating, Al-HTCMC is able to spread the liquid to cover the entire surface for all flow rates.

7.4 Recommendations

1. If mixture of powder and binder can be sprayed over the plain surface, coating fabrication can be much easier and better controlled. So, spraying system should be pursued to spread the mixture of powder and binder on the plain surface prior to brazing process.
2. Coating should be developed using smaller brazing particles when its thickness is needed to be thinner than produced in this study.
3. Long term reliability test must be conducted for all microporous coatings presented in this study.
4. Spray cooling tests should be conducted to CHF using heaters with higher power ratings (>250 W).

APPENDIX A

POROSITY MEASUREMENT

A.1 Porosity Measurement

Porosity was measured using image processing technique from multiple cross-section images of a coating. Porosity was measured as ratio of void area to total area. MatLab codes, used to evaluate the porosity, determines the void area by its color (grey or black) and divides it by the total area of the cross-section. An example of cross-sectional image used for image processing is shown in Figure A.1, which is cropped at the bottom of the coating near the substrate and at the top of the coating. More than 20 images were used for the same coating out of four different samples and the porosity values were averaged.

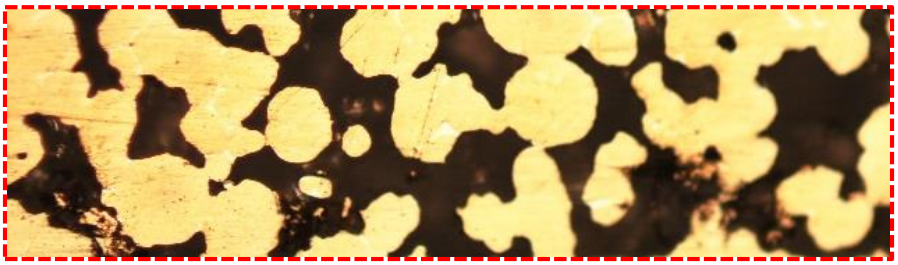

Figure A.1 Cropped cross-sectional image of Cu-HTCMC

MatLab codes:

```
function data=porosity_measurement

imagelist = dir('*.jpg');
N = numel(imagelist);
imdata = cell(1, numel(imagelist));
data=zeros(N,1);

for k = 1: N
   imdata{k} = imread(imagelist(k).name);
   Igray=rgb2gray(imdata{k});
   Ibw=im2bw(Igray);
   Vv=bwarea(~Ibw);
   Vt=Vv+bwarea(Ibw);
   data(k,1)=Vv/Vt;
   end
xlswrite('data.xls',data);
```

APPENDIX B

ADDITIONAL EXPERIMENTAL DATA

B.1 Cu-Microporous vs. Al-Microporous coatings in Pool Boiling of Acetone and HFE-7100

In order to compare the pool boiling performance of Al-HTCMC with copper microporous coating in acetone and HFE-7100, Cu-HTCMC is tested in saturated acetone and a pool boiling data of copper microporous coating in saturated HFE-7100 is obtained from [28]. All the tests, including that in [28], are conducted with identical heater size and test conditions but note that Al-HTCMC is tested on aluminum block while copper microporous coatings are tested on copper block. Figure B.1 displays the pool boiling performances of Al-HTCMC and Cu-HTCMC in saturated acetone and Figure B.2 shows the pool boiling performances of Al-HTCMC and Cu-microporous coating [28]. For both fluids, acetone and HFE-7100, the figures conclude that despite the difference in thermal conductivity, Al-HTCMC enhances boiling heat transfer as much as copper microporous coatings and even more in CHF.

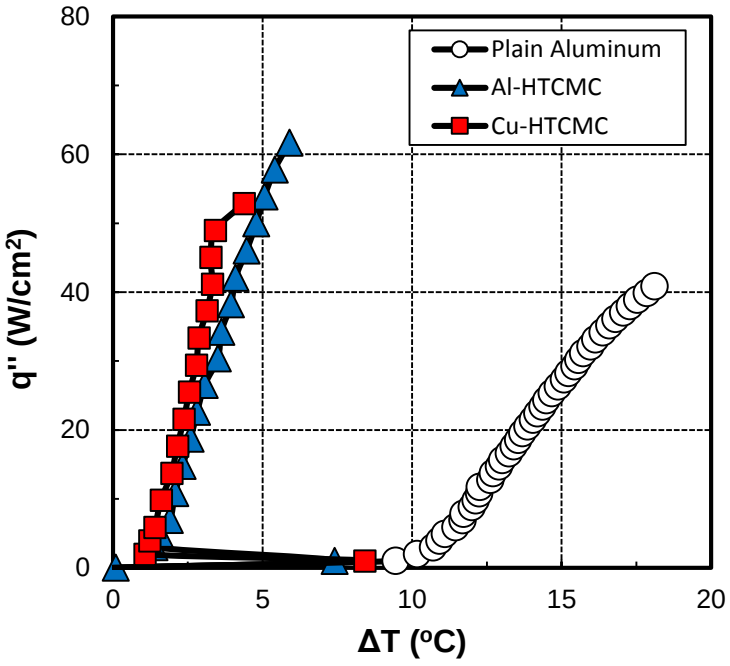

Figure B.1 Comparison of pool boiling performances of Cu-HTCMC and Al-HTCMC in saturated acetone

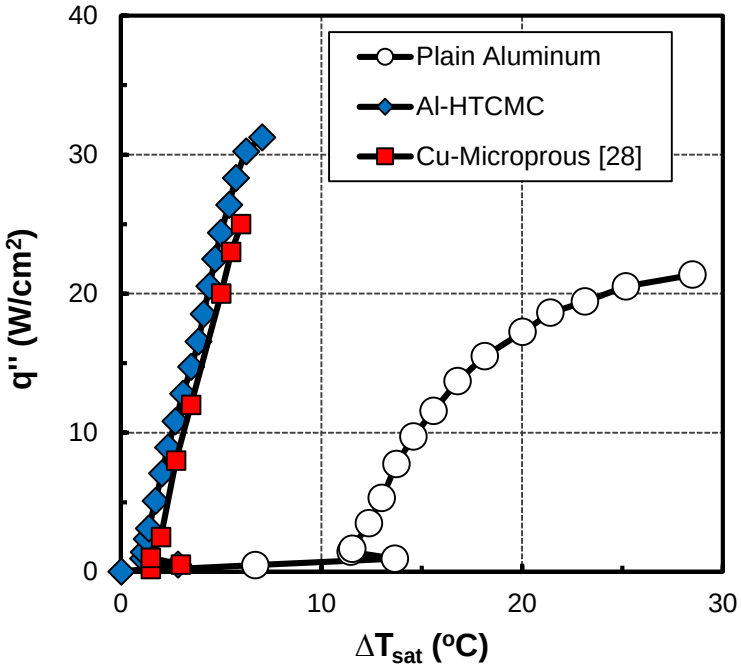

Figure B.2 Comparison of pool boiling performances of Cu-Microporous [28] and Al-HTCMC in saturated HFE-7100

REFERENCES

[1] O'Connor, J. P. and You, S. M., 1995, “A Painting Technique to Enhance Pool Boiling Heat Transfer in FC-72,” Journal of Heat Transfer, Vol. 117, No. 2, pp. 387-393

[2] Rainey, K. N. and You, S. M., 2000, “Pool Boiling Heat Transfer From Plain and Micro-porous, Square Pin Finned Surfaces in Saturated FC-72", ASME Journal of Heat Transfer, 122, pp. 509-516.

[3] Kim, J. H., 2006, "Enhancement of Pool Boiling Heat Transfer Using Thermally Conductive Microporous Coating Techniques." PhD Thesis, UT Arlington.

[4] Trautman, M. A., Tirumala, M., and You, S. M., 2008, “Investigation of Microporous Coatings and Mesoscale Evaporator Enhancements for Two-Phase Cooling of Electronic Components”, Journal of Electronic Packaging, 130, pp. 11007-1 - 11007-6

[5] Semenic, T., and You. S. M., 2011, “Two-phase Heat Sinks with Microporous Coating”, 9th Int. Conference on Nanochannels, Microchannels, and Minichannels, Edmond, CA

[6] Moreno, G., 2009, “Experminental Inverstigation of Flow Boiling and Spray Cooling on Enhanced Surfaces in FC-72”, PhD Thesis, UT Arlington.

[7] Li, Chen and Peterson, G. P., 2007 "Parametric Study of Pool Boiling on Horizontal Highly Conductive Microporous Coated Surfaces,” Journal of Heat Transfer, 129, pp. 1465-1475.

[8] 3M Product Brochure, 2008, 3M Micro-porous Metallic Boiling Enhancement Coating (BEC) L-20227.

[9] Tong, W., Bar-Cohen, A., Simon, T. W., and You, S. M., 1990, “Contact Angle Effects on Boiling Incipience of Highly-Wetting Liquids”, Int. Journal of Heat and Mass Transfer, 33(1), pp. 91-103.

[10] Carey, Van P. Liquid-Vapor Phase-Change Phenomena. 2nd. New York: Taylor & Francis, 2008.

[11] You, S. M, Rainey, K.N., and Ammerman, C. N., 2004, “A New Microporous Surface Coating for Enhancement of Pool and Flow Boiling Heat Transfer”, Advances in Heat Transfer, 38, pp. 73-142.

[12] Rohsenow, W. M., 1962, “A Method of Correlating Heat Transfer Data for Surface Boiling of Liquids,” Journal of Heat Transfer, Vol. 84, pp. 969-975.

[13] Mostinski, I.L., 1963, “Application of the Rule of Corresponding States for Calculation of Heat Transfer and Critical Heat Flux to Boiling Liquids,” British Chemical Engineering Abstracts: FOLIO no. 150, 580.

[14] Zuber, N., 1959, “Hydrodynamic Aspects of Boiling Heat Transfer,” AEC Report No. AECU-4439, Physics and Mathematics.

[15] Lienhard, J. H., Dhir, V. K. and Riherd, D. M., 1973, "Peak Pool Boiling Heat Flux Measurements on Finite Horizontal Flat Plate," J. Heat transfer, 95, pp. 477-482.

[16] Bergles, A. E., and Chyu, M. C., 1982, "Characteristics of Nucleate Pool Boiling From Porous Metallic Coatings." J. Heat Transfer, Vol. 104, pp. 279-285.

[17] Thome, J. R., 1992, “Mechanisms of Enhanced Nucleate Pool Boiling,” *Proceedings of the Engineering Foundation Conference on Pool and External Flow Boiling*, ASME, New York, pp. 337-343.

[18] Malyshenko, S. P., 1991, "Features of heat transfer with boiling on surfaces with porous coatings." Thermal Engineering, Vol. 38, no. 2, pp. 81-88.

[19] Milton, R. M., May. 21, 1968, “Heat Exchange System", U.S. Patent 3,384,154.

[20] O'Neill, P. S., Gottzmann, C. F., and Minton, P. E., 1973, “High Efficiency Heat Exchangers", Chem. Eng. Progr., 69, No. 7, pp. 69-75.

[21] Almgren, D. W. and Smith, J. L., Jr., 1969, “The Inception of Nucleate Boiling with Liquid Nitrogen", J. Eng. Ind. Trans. ASME Series B, 91, pp. 1210-1216.

[22] Dyundin, V. A., Danilova, G. N., Borishanskaya, A. V., Krotkov, V. N., Gogolin, V. A., Vakhalin, V. A., and Protasov, G. A., 1975, “Enhancement of Heat Transfer with Boiling Refrigerants on Coated Surfaces", Khim. Neft. Mashinostr, 9, pp. 22-23.

[23] Inoue, K., Jul. 23, 1974, “Heat Exchanger", U.S. Patent 3,825,064.

[24] Albertson, C. E., Apr. 19, 1977, “Boiling Heat Transfer Surface and Method", U.S. Patent 4,018,264.

[25] Trepp, C. H. and Hooman, T. V., 1980, “Boiling Heat Transfer from Structured Surfaces to Liquid Nitrogen", Warme-und Stoubertragung, 14, pp. 15-22.

[26] Chang, J. Y. and You, S. M., 1996, \Heater Orientation Effects on Pool Boiling of Micro-Porous-Enhanced Surfaces in Saturated FC-72", ASME Journal of Heat Transfer, 118, pp. 937-943.

[27] Hwang, G.S. and Kaviany, M., 2006, “Critical Heat Flux in Thin, Uniform Particle Coatings,” International Journal of Heat Transfer, 49, pp. 844-849.

[28] Thiarajan et al., 2010, "Enhancement of Heat Transfer with Pool and Spray Impingement Boiling on Micro-porous AND Nanowire Surface Coatings," International heat transfer conference, Washington DC, IHTC14-23284.

[29] Kline, S. J. and McClintock, F. A., 1953, “Describing Uncertainties in Single-Sample Experiments,” Mechanical Engineering, Vol. 75, No. 1, pp. 3-8.

[30] Kwark, S. M., 2009, “Pool Boiling Heat Transfer Characteristics of Nanofluids and Nanocoatings,” PhD Thesis, UT Arlington.

[31] Takata, Y., Hidaka, S., Masuda, M. and Ito, T., 2003, “Pool Boiling on a Superhydrophilic Surface”, Int. J. Energy Res., 27, pp.111-119.

[32] Malla, S., 2014, “Experimental Investigation of Nucleate Boiling and Thin-Film Evaporation on Enhanced Silicon Surfaces”, PhD Thesis, UT Arlington.

[33] Kim, J. H. Rainey, K. N., You, S. M., and Park, J. Y., 2002, “Mechanism of Nucleate Boiling Heat Transfer Enhancement From Microporous Surfaces in Saturated FC-72,” Journal of Heat Transfer, Vol. 124, No. 3, pp. 500-506.

[34] Chang, J. Y. and You, S. M., 1997, “Enhanced Boiling Heat Transfer from Microporous Surfaces: Effects of a Coating Composition and Method,” International Journal of Heat and Mass Transfer, Vol. 40, No. 18, pp. 4449-4460.

[35] Rao, G. V. and Balakrishnan, A. R., “Heat Transfer in Nucleate Pool Boiling of Multicomponent Mixtures,” Experimental Thermal and Fluid Science, vol. 29, pp. 87-103, 2004.

[36] Kutateladze, S. S., and Gogonin, I. I., 1977, “Critical Heat Flux as a Function of Heater Size for Liquid Boiling in Large Enclosure”, Journal of Engineering Physics, 33, pp. 1286-1289.

[37] Coursey, J. S., Kim, J. G., Kiger, K. T., 2007, “Spray Cooling of High Aspect Ratio Open Microchannels”, Journal of Heat Transfer, 129, pp. 1052-1059.

[38] Yang, J., Chow, L. C., and Pais, M. R., 1996, “Nucleate Boiling Heat Transfer in Spray Cooling”, J. Heat Transfer, 118, pp. 668-671.

[39] Hsieh, C. C., and Yao, S. C., 2006, "Evaporative Heat Transfer Characteristics of a Water Spray on Micro-Structured Silicon Surfaces," Int. Journal of Heat and Mass Transfer, 49(5-6), pp. 962-974.

[40] Horacek, B., Kiger, K. T., and Kim, J., 2005, "Single Nozzle Spray Cooling Heat Transfer Mechanisms," Int. Journal of Heat and Mass Transfer, 48(8), pp. 1425-1438.

[41] Ndao, S., Lee, H. J., Peles, Y. and Jensen, M. K., 2012, “Heat Transfer Enhancement from Micro Pin Fins Subjected to an Impingement Jet”, Int. Journal of Heat and Mass Transfer, 55, pp. 413-421.

[42] Yang, B.H., Wang, H., Zhu, S., Liao, Q., Ding, Y.D. and Chen, R., 2013, “Heat Transfer Enhancement of Spray Cooling with Ammonia by Microcavity Surfaces”, Applied Thermal Engineering, 50(1), pp. 245-250.

[43] Kim, J. H., You, S.M., and Choi, S., 2008, “Evaporative Spray Cooling of Plain and Microporous Coated Surfaces”, Int. Journal of Heat and Mass Transfer, 47, pp. 3307-3315.

[44] Estes, K. A. and Mudawar, I. 1995, "Correlation of Sauter Mean Diameter and Critical Heat Flux for Spray Cooling of Small Surfaces," Int. Journal of Heat and Mass Transfer, vol. 38, pp. 2985-2996.

BIBLIOGRAPHICAL INFORMATION

Ajay Gurung completed his Bachelors of Science in Mechanical Engineering at University of Texas at Arlington in December 2008. He then joined Micro-Scale Heat Transfer Laboratory at University of Texas at Arlington for his Ph.D. His research of interests includes two phase heat transfer enhancement, and thermal management of microelectronics.